

TOPICAL REVIEW

Research progress of femtosecond surface plasmon polariton^{*}

To cite this article: Yulong Wang *et al* 2020 *Chinese Phys. B* **29** 027302

View the [article online](#) for updates and enhancements.

Recent citations

- [Plasmonic tweezers: for nanoscale optical trapping and beyond](#)
Yuquan Zhang *et al*
- [Enhanced circular dichroism of TDBC in a metallic hole array structure](#)
Tiantian He *et al*
- [Effect of recombination process in femtosecond laser-induced modification on Ge crystal](#)
Jia-Qi Ju *et al*

Research progress of femtosecond surface plasmon polariton*

Yulong Wang(王玉龙)¹, Bo Zhao(赵波)², Changjun Min(闵长俊)^{1,†}, Yuquan Zhang(张聿全)¹,
Jianjun Yang(杨建军)², Chunlei Guo(郭春雷)², and Xiaocong Yuan(袁小聪)^{1,‡}

¹Nano Photonics Research Centre, Shenzhen Key Laboratory of Micro-Scale Optical Information Technology,
Shenzhen University, Shenzhen 518060, China

²The Guo China-US Photonics Laboratory, State Key Laboratory of Applied Optics, Changchun Institute of Optics,
Fine Mechanics and Physics, Chinese Academy of Sciences, Changchun 130033, China

(Received 31 October 2019; revised manuscript received 14 December 2019; accepted manuscript online 3 January 2020)

As the combination of surface plasmon polariton and femtosecond laser pulse, femtosecond surface plasmon polariton has both nanoscale spatial resolution and femtosecond temporal resolution, and thus provides promising methods for light field manipulation and light-matter interaction in extreme small spatiotemporal scales. Nowadays, the research on femtosecond surface plasmon polariton is mainly concentrated on two aspects: one is investigation and characterization of excitation, propagation, and dispersion properties of femtosecond surface plasmon polariton in different structures or materials; the other one is developing new applications based on its unique properties in the fields of nonlinear enhancement, pulse shaping, spatiotemporal super-resolved imaging, and others. Here, we introduce the research progress of properties and applications of femtosecond surface plasmon polariton, and prospect its future research trends. With the further development of femtosecond surface plasmon polariton research, it will have a profound impact on nano-optoelectronics, molecular dynamics, biomedicine and other fields.

Keywords: surface plasmon polariton, femtosecond laser pulse, spatiotemporal super-resolution, nonlinear optics

PACS: 73.20.Mf, 42.65.Re, 42.65.Sf

DOI: 10.1088/1674-1056/ab6717

1. Introduction

In recent years, with the rapid development of information technology and the growing demands for integrated micro-/nanoscale photonic devices, manipulation of photon in extremely small spatiotemporal scale is urgently needed. Spatially, surface plasmon polariton (SPP), as an optical surface wave mode with ability of breaking the traditional optical diffraction limit, can provide not only nanoscale spatial resolution, but also a tremendously enhanced local electromagnetic (EM) field. Since Ebbesen *et al.*^[1] first reported the SPP-related extraordinary transmission phenomenon through sub-wavelength hole arrays, SPP provides a new platform for highly integrated and efficient nanoscale photonic devices, and shows broad application prospects in optical storage, photocatalysis, optical sensing, optical tweezers, Raman scattering, *etc.* In terms of time-scale, the rapidly developing femtosecond laser is useful for exploring ultrafast dynamic processes happened in the fields of physical, chemical and biological, as well as some high-intensity and nonlinear optical phenomena, due to its ultrashort pulse duration (10^{-15} s) and ultrahigh peak power. Meanwhile, femtosecond SPP pulses excited by

femtosecond laser may both have nanoscale spatial resolution and femtosecond-scale temporal resolution, which provides an effective approach for light field manipulation in an extremely small spatiotemporal scale and research on light-matter interaction.

Recently, femtosecond SPP has become a new cross-over research area between nanophotonics and ultrafast optics. The characteristics of femtosecond SPP such as excitation, diffusion, dispersion, local enhancement and spin-orbital angular momentum, and its applications in fields as nonlinear enhancement, on-chip optical manipulation, optical tweezers and super spatiotemporal resolution imaging, have attracted extensive attention and achieved many innovative results with great influences.

This paper introduces the research progress of femtosecond SPP. The basic mechanism of SPP is outlined in Section 2, the research advancements on spatiotemporal physical characteristics of femtosecond SPP are highlighted in Section 3, and the latest application researches of femtosecond SPP in nonlinear enhancement, on-chip optical manipulation, super spatiotemporal resolution imaging are described in Sections 4.

*Project supported by the National Natural Science Foundation of China (Grant Nos. 91750205, 61427819, U1701661, 11674178, and 61975128), the Leading Talents of Guangdong Province Program, China (Grant No. 00201505), the Natural Science Foundation of Guangdong Province, China (Grant Nos. 2016A030312010 and 2017A030313351), the Science and Technology Innovation Commission of Shenzhen City (Grant Nos. JCYJ20180507182035270, KQTD2017033011044403, KQJSCX20170727100838364, ZDSYS201703031605029, and JCYJ2017818144338999), and the K. C. Wong Education Foundation (Grant No. GJTD-2018-08).

[†]Corresponding author. E-mail: cjmin@szu.edu.cn

[‡]Corresponding author. E-mail: xcyuan@szu.edu.cn

Finally, we make a summary of femtosecond SPP research and look forward to the future development trend.

2. Basic mechanism of SPP

SPP is a localized EM wave mode generated by collective resonance of free electrons with the incident photons on metal surfaces,^[2] and propagates within subwavelength range of the metal surface. It can be used to break the traditional optical diffraction limit and generate highly localized nanoscale light fields as its wavelength is shorter than that of the incident light.^[3] For example, a gap mode can be formed in the gap region between noble metal nanoparticles (NPs)/nanoprobes and metal film through the interaction between the excited SPP and the localized surface plasmon (LSP) mode of metal NPs or nanoprobes,^[4] resulting in the highly confined electric field with spatial scale smaller than that of the NPs or nanoprobes, so as to achieve nanoscale imaging resolution. In addition, SPP also has the property of near-field energy enhancement, which can concentrate the energy of incident light within nanoscale volume, thus increasing the enhancement factor (EF) of near-field EM field to the order of 10^4 ,^[5]

and greatly enhance the Rayleigh/Raman scattering signals and nonlinear optical signals. At present, such technologies as surface-enhanced Raman scattering (SERS)^[6–9] and tip-enhanced Raman scattering (TERS)^[10–14] resulted from combination of SPP with metal NPs or nanoprobes have been widely applied in the fields of molecular spectrum detection and imaging, *etc.*

2.1. Dispersion characteristics of SPP

In order to study the dispersion characteristics of SPP, we can start from the optical characteristics of metals,^[15,16] and obtain the SPP dispersion formula at the dielectric–metal interface by solving Maxwell's equations. Figure 1(a) shows a classical two-dimensional (xz -plane) model, including isotropic media ($z > 0$) and metal ($z < 0$) with dielectric constants ϵ_1 and ϵ_2 . The dielectric constant of metal is generally made up of a negative real part ϵ_r and a positive imaginary part ϵ_i , and denoted as $\epsilon_2 = \epsilon_r + i\epsilon_i$. Since it has been proved that SPP can be excited only by light with transverse-magnetic (TM) polarization mode,^[15] the EM field distribution in the dielectric and metal zones is shown as follows:

$$\begin{aligned} H_1(x, z, t) &= (0, A, 0) \exp(ik_{1x}x - k_{1z}z - i\omega t), \\ E_1(x, z, t) &= \frac{iA}{\omega\epsilon_0\epsilon_1} (k_{1z}, 0, ik_{1x}) \exp(ik_{1x}x - k_{1z}z - i\omega t), \quad (z > 0), \end{aligned} \quad (1)$$

$$\begin{aligned} H_2(x, z, t) &= (0, B, 0) \exp(ik_{2x}x + k_{2z}z - i\omega t), \\ E_2(x, z, t) &= -\frac{iB}{\omega\epsilon_0\epsilon_2} (k_{2z}, 0, -ik_{2x}) \exp(ik_{2x}x + k_{2z}z - i\omega t), \quad (z < 0), \end{aligned} \quad (2)$$

where H_1 and E_1 (H_2 and E_2) are the magnetic field and electric field components in the dielectric (metal), respectively, t is the propagation time of EM wave in the dielectric (metal), ϵ_0 is the permittivity of vacuum, ω is the angular frequency of incident laser, A and B are constants. The wave vector components of EM waves parallel to and perpendicular to the interface in the dielectric (metal) region are respectively represented by k_{1x} and k_{1z} (k_{2x} and k_{2z}), where $k_{1z} = \sqrt{k_{1x}^2 - \epsilon_1 k^2}$ ($k_{2z} = \sqrt{k_{2x}^2 - \epsilon_2 k^2}$, $k = \omega/c$ is free-space wave vectors, and c is the velocity of light in vacuum). Considering that the components H_y and E_x at the dielectric–metal interface are continuously variable, the following equations can be obtained:

$$A = B, \quad k_{1x} = k_{2x} = k_{\text{SPP}}, \quad Ak_{1z}/\epsilon_1 = -Bk_{2z}/\epsilon_2, \quad (3)$$

where k_{SPP} is the wave vector of SPP. The functional relation between k_{1z} and k_{2z} can be obtained from Eq. (3) under the excitation of TM mode

$$k_{1z}/\epsilon_1 = -k_{2z}/\epsilon_2. \quad (4)$$

Substituting Eq. (4) into Eq. (3), we can get the dispersion

relation of SPP excited at the dielectric–metal interface as

$$k_{\text{SPP}} = k \sqrt{\epsilon_1 \epsilon_2 / (\epsilon_1 + \epsilon_2)} = \frac{\omega}{c} \sqrt{\epsilon_1 \epsilon_2 / (\epsilon_1 + \epsilon_2)}. \quad (5)$$

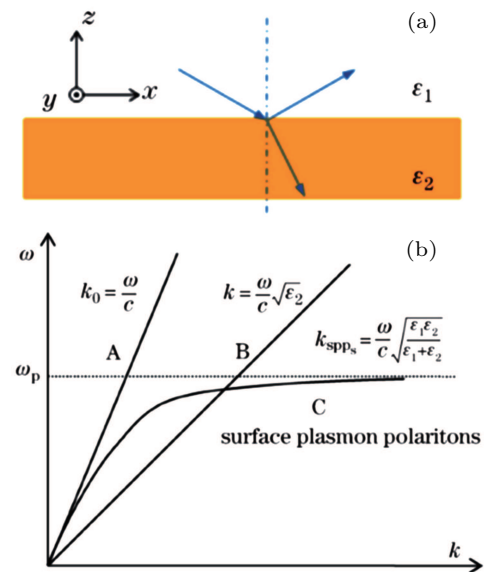


Fig. 1. (a) Schematic diagram of SPPs excited on the medium–metal interface. (b) Dispersion curve of an SPP wave, k_{SPP} and k are the SPP and free-space wave vectors, respectively.^[16]

In Fig. 1(b) we can observe that the SPP dispersion curve has a nonlinear characteristic. For a given frequency, the wave vector of SPP (k_{SPP}) is always larger than that of the incident light in free-space, causing wave vector mismatch between the incident light and SPP. Therefore, SPP can never be directly excited by the incident light until the wave vector of the incident light is compensated by special methods.

Since SPP is an evanescent field, its EM field component perpendicular to the interface exponentially decays with the increase of distance in the dielectric (metal). When the energy decays to $1/e$ of the initial value, the distance is called penetration depth, denoted as δ_1 (δ_2):

$$\delta_{1,2} = \frac{1}{k} \left| \frac{\epsilon_1 + \epsilon_2}{-\epsilon_{1,2}^2} \right|^{1/2}. \quad (6)$$

As Ohmic loss of a metal is determined by the imaginary part of dielectric constant, the energy of SPP wave decays exponentially as it propagates horizontally along the dielectric-metal interface. When the energy decays to $1/e$ of the initial value, the propagation distance is called the propagation length (L_{SPP}), which can be expressed as:

$$L_{\text{SPP}} = \frac{1}{2\text{Im}k_{\text{SPP}}} = \frac{c}{\omega} \left(\frac{\epsilon_1 + \epsilon_2}{\epsilon_1 \epsilon_2} \right)^{3/2} \frac{\epsilon_r^2}{\epsilon_1}. \quad (7)$$

Besides the semi-infinite medium-metal interface, SPP can also be excited and propagate in multilayer structures, and show different dispersion relations. When there are multilayers consisting of alternating conducting and dielectric films, as each interface can sustain bound SPP, they will interact with each other and form coupled mode once the distance between

adjacent interfaces is close to or less than the decay length. To introduce the dispersion characteristics of SPP in multilayers, here we take two specific three layer structures as examples, including the insulator/metal/insulator (IMI) heterostructure and metal/insulator/metal (MIM) heterostructure. The geometry of a three-layer structure is shown in Fig. 2(a).

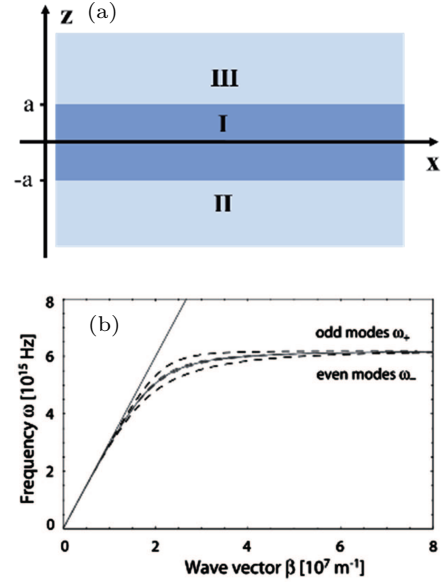


Fig. 2. (a) Geometry of a three-layer system consisting of a thin layer I with width of $2a$ sandwiched between two infinite half spaces II and III. (b) Dispersion relation of the coupled odd and even modes for an air/silver/air multilayer with a metal core of thickness 100 nm.^[17]

Since we only interested in the lowest-order bound modes, we give a general description of TM modes that are non-oscillatory in the z direction by solving Maxwell's equations. For $z > a$, $z < -a$, and $-a < z < a$ regions, the EM fields are^[17]

$$\begin{aligned} H_3(x, z, t) &= (0, C, 0) \exp(ik_{3x}x - k_{3z}z - i\omega t), \\ E_3(x, z, t) &= \frac{iC}{\omega\epsilon_0\epsilon_3} (k_{3z}, 0, ik_{3x}) \exp(ik_{3x}x - k_{3z}z - i\omega t), \quad (z > a), \end{aligned} \quad (8)$$

$$\begin{aligned} H_2(x, z, t) &= (0, D, 0) \exp(ik_{2x}x + k_{2z}z - i\omega t), \\ E_2(x, z, t) &= -\frac{iD}{\omega\epsilon_0\epsilon_2} (k_{2z}, 0, -ik_{2x}) \exp(ik_{2x}x + k_{2z}z - i\omega t), \quad (z < -a), \end{aligned} \quad (9)$$

$$\begin{aligned} H_1(x, z, t) &= (0, M, 0) \exp(ik_{1x}x + k_{1z}z - i\omega t) + (0, N, 0) \exp(ik_{1x}x - k_{1z}z - i\omega t), \\ E_1(x, z, t) &= -\frac{iM}{\omega\epsilon_0\epsilon_1} (k_{1z}, 0, ik_{1x}) \exp(ik_{1x}x + k_{1z}z - i\omega t) \\ &\quad + \frac{iN}{\omega\epsilon_0\epsilon_1} (k_{1z}, 0, ik_{1x}) \exp(ik_{1x}x - k_{1z}z - i\omega t), \quad (-a < z < a), \end{aligned} \quad (10)$$

where C , D , M , and N are constants. Considering that the components H_y and E_x at the dielectric-metal interface are continuously variable, yielding

$$\begin{aligned} k_{1x} &= k_{3x} = k_{\text{SPP}}, \quad C \exp(-k_{3z}a) = M \exp(k_{1z}a) + N \exp(-k_{1z}a), \\ \frac{C}{\epsilon_3} k_{3z} \exp(-k_{3z}a) &= -\frac{M}{\epsilon_1} k_{1z} \exp(k_{1z}a) + \frac{N}{\epsilon_1} k_{1z} \exp(-k_{1z}a) \end{aligned} \quad (11)$$

at $z = a$ and

$$k_{1x} = k_{2x} = k_{\text{SPP}}, \quad D \exp(-k_{2z}a) = M \exp(-k_{1z}a) + N \exp(k_{1z}a),$$

$$\frac{D}{\epsilon_3} k_{2z} \exp(-k_{2z}a) = -\frac{M}{\epsilon_1} k_{1z} \exp(-k_{1z}a) + \frac{N}{\epsilon_1} k_{1z} \exp(k_{1z}a) \quad (12)$$

at $z = -a$, where $k_{jz} = \sqrt{k_{jx}^2 - \epsilon_j k^2}$ ($j = 1, 2, 3$). An implicit expression for the dispersion relationship can be obtained by solving these above equations as

$$\exp(-4k_{1x}a) = \frac{k_{1z}/\epsilon_1 + k_{2z}/\epsilon_2}{k_{1z}/\epsilon_1 - k_{2z}/\epsilon_2} \cdot \frac{k_{1z}/\epsilon_1 + k_{3z}/\epsilon_3}{k_{1z}/\epsilon_1 - k_{3z}/\epsilon_3}, \quad (13)$$

It is found that equation (14) can be simplified to Eq. (4) if the layer I has infinite thickness.

To simplified the model, we consider a special symmetrical case where the dielectric constants of layers II and III are equal, *i.e.*, $\epsilon_2 = \epsilon_3$. In this case, according to the direction of the electric field at the interface between the metal and the dielectric, an odd symmetry or even symmetry modes can be achieved (Fig. 2(b)), and their dispersion relations can be simplified as

$$\tanh(k_{1x}a) = -\frac{\epsilon_1 k_{2z}}{\epsilon_2 k_{1z}}, \quad (14)$$

$$\tanh(k_{1x}a) = -\frac{\epsilon_1 k_{1z}}{\epsilon_2 k_{2z}}. \quad (15)$$

These two dispersion relations can be applied to both IMI and MIM structures to study the properties of the coupled SPP modes, respectively. For the IMI structures, the confinement of the odd modes to the metal film decreases with reducing the thickness of metal film, which means that it can sharply increase the propagation length of SPP, while the even mode leads to exactly the opposite result. For the MIM structures, the fundamental odd mode does not exhibit a cut-off for vanishing core layer thickness, indicating that SPP can propagate in MIM waveguide with deep-subwavelength width. In addition, with a sufficiently small dielectric core layer thickness, a larger propagation constant can be achieved even if the excitation frequency is much smaller than that of the plasma resonance frequency. Thus, it is possible to obtain a larger wave vector while a smaller penetration length into the metal layer, by adjusting the geometry.

2.2. Excitation methods of SPP

Since the dispersion curve of SPP always lies to the right side of dispersion curve of light wave vector in free space, as shown in Fig. 1(b), meaning that there is momentum mismatch between SPP and incident light in free space. Therefore, a compensation for wave vector of the incident light is needed to satisfy the wave vector matching condition which is the indispensable prerequisite for SPP excitation. Generally, several methods such as prism coupling (Kretschmann and Otto configurations), optical grating diffraction and near-field scattering configuration can be used to compensate the wave vector

to excite SPP. These common SPP excitation methods are described as follows.

2.3. Excitation of SPP through prism coupling

The Kretschmann configuration is composed of a dielectric prism with high refractive index and a thin metal film coated on its surface. As shown in Fig. 3(a), the laser enters the metal film at an angle larger than the critical angle of total internal reflection,^[18,19] and the wave vector of the incident light is increased by virtue of the high refractive index of the dielectric prism. SPPs are excited at the metal/air interface, and there is

$$k_{\text{SPP}} = k \sqrt{\epsilon_{\text{prism}}} \sin(\theta). \quad (16)$$

If an additional dielectric layer with refractive index lower than that of the prism is deposited between the prism and metal film, as shown in Fig. 3(b), the SPP can be excited at the upper or the lower surfaces of metal film, respectively, by changing the incident angle, due to the fact that the additional layer can provide a necessary compensation of the wave vector for resonant excitation of SPP.

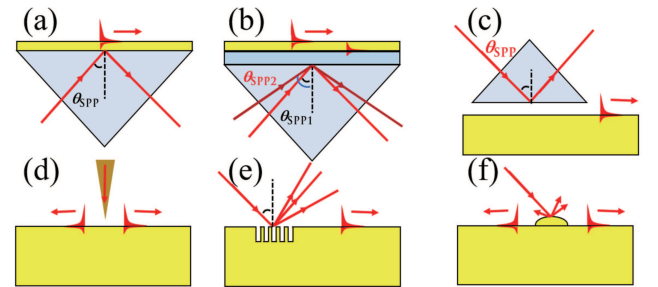


Fig. 3. SPP excitation configurations: (a) Kretschmann geometry, (b) two-layer Kretschmann geometry, (c) Otto geometry, (d) excitation with a metal tip, (e) diffraction on a grating, (f) diffraction on surface features.^[15]

As the Kretschmann configuration cannot be used to excite SPP on the surface of a thick metal film or a lump metal, Otto proposed the Otto configuration of dielectric prism inverted on the metal film (Fig. 3(c)), to excite SPP on the air-metal interface through photonic tunneling effect generated in the air gap between the prism and the metal surface.^[20] The resonance condition of this configuration is similar to the Kretschmann configuration with a two-layer film.

2.3.1. Excitation of SPP through grating diffraction

If a periodic grating is etched on a metal surface, an extra wave vector compensation is introduced for satisfying the wave vector matching condition of exciting SPPs, as shown in Fig. 3(e). The wave vector matching condition for a periodic grating to excite SPP is^[15]

$$\text{Re}(k_{\text{SPP}}) = \text{Re}\left(\frac{\omega}{c} n_0 \sin(\theta) \pm m \frac{2\pi}{\Lambda}\right), \quad (17)$$

where n_0 is the refractive index of material near metal surface, Λ is the period of grating, and m is the diffraction order (a natural number in general). This method is featured by high efficiency of SPP excitation, however, it has high fabrication cost and is difficult in dynamic controlling.

2.3.2. Excitation of SPP through near-field scattering

The near-field scattered waves generated by a subwavelength structure such as nanoprobe, nanoparticle (NP) or surface defect have various spatial wave vectors that covers a large range,^[15] parts of these could meet the wave vector matching condition, resulting in SPP waves generation. In the near-field range, the size of probe apex is always far less than the wavelength of incident light, then the tunneling effect occurs on the metal surface when the incident light irradiates the nanoprobe, leading to the generation of evanescent waves, which provide necessary wave vector compensation to excite SPP near the apex,^[21] as shown in Fig. 3(d). In addition, if an NP was placed on a metal surface, a similar scattering excitation effect can be achieved,^[22] as shown in Fig. 3(f). This SPP excitation method has an advantage of very simple structure, however, only a very small part of the scattered light can fit the wave vector matching condition, resulting in extremely low SPP excitation efficiency.

3. Research progress on spatiotemporal characteristics of femtosecond SPP

Since Maiman invented the world's first laser (ruby laser) in 1960,^[23] laser technology has undergone decades of development, and the pulse duration has been gradually compressed down to femtosecond-scale.^[24–28] Femtosecond laser, like a ruler accurate enough in time, can be well used to explore ultrafast phenomena and characterize the dynamic evolution processes of physical and chemical events,^[29] such as molecular structure dynamics,^[30] ultrafast photosynthesis process,^[31] molecular stimulated Raman scattering (SRS),^[32] and thus was awarded the Nobel Prize due to Prof. Zewail's pioneering work.^[33] Another excellent property of femtosecond laser is the ultrahigh peak power, which makes it be widely used in femtosecond laser filamentation,^[34,35] attosecond pulse generation and detection,^[36–38] ultrafast nonlinear optics,^[39,40] high harmonic generation (HHG)^[5,41] and femtosecond optical trapping,^[42,43] *etc.* In addition, under the immediate demand for exploring ultrafast processes such as chemical reactions and photosynthesis, femtosecond-scale temporal resolution imaging technology comes into being, and gradually becomes a common means in studying ultrafast process.^[44–47]

With the development of femtosecond laser technology, people combined the femtosecond laser and SPP to generate ultrafast SPP pulses. Considering the nanoscale spatial resolution and local EM field enhancement effect of SPP, and the

femtosecond-scale temporal resolution characteristics and ultrahigh peak power of femtosecond laser pulse, it is possible to achieve optical detection and imaging with super spatiotemporal resolution when combining these advantages. Moreover, the combination of SPP and femtosecond laser pulse can greatly strengthen various nonlinear optical effects, generate lots of novel physical phenomena, and bring in new applications. At present, researchers have paid much attention on characterization of femtosecond SPP pulses, and conducted extensive researches. The study on femtosecond SPP characteristics includes excitation and propagation characteristics on metal film, surface structures and nanoprobe, and spinning and orbital angular momentum interaction characteristics, *etc.* These aspects will be introduced respectively as follows.

3.1. The excitation and propagation characteristics of femtosecond SPP on metal film or surface structure

SPP mode propagating along the surface of a metal film can be generated with proper incident light and wave vector matching structure. Yet, how to excite SPP pulse with broadband spectrum is one of the current research hotspots. In 2008, Yalcin *et al.* investigated the spectral bandwidth and phase shift effect of resonant excitation of femtosecond SPP pulse on metal film based on Kretschmann configuration.^[48] They found that the resonant excitation causes the spectrum narrowing and phase shifting, resulting in the time domain broadening of SPP pulses. The angular dependence characteristics of femtosecond SPP pulse excited by ultrashort laser pulse at the metal film/air interface are obtained by measuring reflected femtosecond laser spectra at different incident angles, as shown in Fig. 4(a). The coupling process of photons and SPP waves only takes place in limited spectral bandwidths. In principle, temporal broadening of SPP pulses can be restrained by compensating the narrowed spectrum and phase shift.

Femtosecond SPP pulses excited on metal films with different materials have different propagation characteristics. Based on this, in 2011, Sámson *et al.* compared the pulse shaping effect and nonlinear propagation modes of ultrafast SPP excited by different metal (Al, Ag, and Au) films with silicon waveguide substrate,^[49] and achieved the effect of group velocity dispersion (GVD) and loss of dispersion (LD) on ultrashort SPP pulses transmission, as shown in Fig. 4(b). Due to the comprehensive effect of GVD and LD, SPP pulses on Al film surface were compressed in the visible spectrum, and obviously broaden in the near-infrared (NIR) band, while the SPP pulses on Ag film surface were somewhat extended from visible to NIR band, and the SPP pulses on Au film surface had a series of obviously compressed and broadened in the visible light range. This work indicated that soliton, self-focusing, self-compression and other effects can be achieved by using the nonlinear SPP metal waveguides.

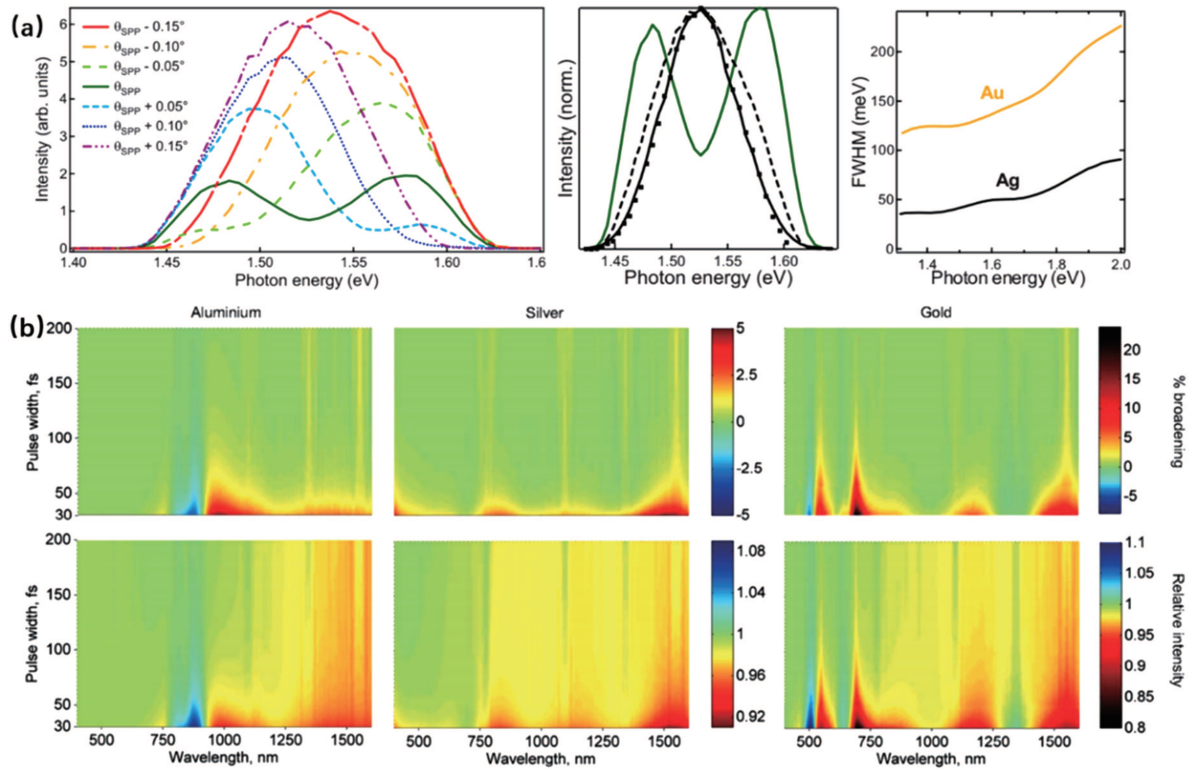


Fig. 4. (a) Spectra of reflected femtosecond laser pulses at different incidence angles (left), comparison of scattered SPP pulse spectrum (black line), incident pulse spectrum (dashed line), reflected pulse spectrum at optimal SPP coupling angle (green line), and difference spectrum (square markers) between incident and reflected pulse spectra (middle), spectral bandwidth (FWHM) of the SPP excitation by prism coupling for Au films (orange line) and Ag films (black line) (right).^[48] (b) Combined impact of group velocity and loss dispersion on SPP pulse transmission over one propagation length on Al, Ag, and Au/silica waveguides: Upper plots show total (GVD- plus LD-induced) percentage pulse broadening; lower plots show normalized output pulse intensity, as functions of input pulse duration and center wavelength.^[49]

In order to further modulate femtosecond SPP on metal films, researchers proposed to fabricate micro-/nanoscale structures on metal film, such as nano-slit, nanodot and nano-step. For example, if slits were etched on a metal film, the SPP wave will be strongly restricted in the cross-sectional direction of the slits, so that it can only propagate in a specific direction. In addition, if structures such as periodically arranged nanodot arrays were fabricated on a metal film, the propagation properties of SPP waves including velocity, dispersion, GVD, diffraction and interference will be modulated to generate new physical phenomena. To study and represent these novel phenomena, the combination of femtosecond-scale temporal resolution technology with microscopic technology becomes a useful access to explore the ultrafast propagation process of SPP. In 2005, Kubo *et al.* investigated the ultrafast process of SPP excited by femtosecond laser pulses (400 nm, 10 fs) on an Ag grating, and achieved the excitation and propagation process of SPP pulses with subwavelength spatial resolution (50 nm) and sub-femtosecond temporal precision (0.33 fs),^[50] by combining interferometric time-resolved two-photon photoemission (ITR-2PP) technology^[51] with photoelectron emission microscopy (PEEM) system.^[52,53] As shown in Fig. 5(a), the coherence polarization excited at different hotspots shift to its own resonant frequency, as the driven pulse weakens, thus leading to a delayed (or advanced) phase and a later (faster) increase of intensity peak corresponding

to the phase of driven field. It provides a new method for research on the dynamic process of ultrafast SPP excited on nanostructures. In 2007, Petek *et al.* successfully combined the temporal resolution of femtosecond spectrograph with the ability of subwavelength imaging of the photoelectron,^[54] and took an external oblique-incident laser on the Ag groove as the excitation source and probe beam of SPP wave packets, so as to generate polarized standing wave at the Ag/vacuum interface through two-path interference. The PEEM was used for imaging the spatial distribution of photoelectron generated through two-photon emission, and the nonlinear graphs of the polarized grating with spatial super-resolution were recorded. 1/4 of the optical period was taken as a step to control the time delay between the pump and probe pulses, and an ultrafast propagation process of SPP wave packet with 60 nm spatial resolution and less than 10-fs temporal resolution was achieved, as shown in Fig. 5(b). This method can be used for imaging the ultrafast process of the coherent field and stimulated carriers of nanoscale optical and electronic structures that could not be observed before. Therefore, it is of great scientific significance.

Besides the research on propagation characteristics of femtosecond SPP pulse, ultrafast evolution process of wave packet is also a hot topic. In 2011, Zhang *et al.* adopted two-photon photoemission photoelectron emission microscopy (2PP-PEEM) system to snapshot the wave packet of femtosec-

ond SPP excited by a single slit etched on an Ag film, and carefully studied the interference process between the incident ultrashort pulse and its excited SPP wave packet.^[55] They found that Fabry–Perot resonance effect was significantly enhanced with the increasing of slit width, and the interference signal could be strengthened by increasing the slit width from sub-wavelength to multiple wavelength. The author used finite-difference time-domain (FDTD) method to simulate the process, and the results consistent with the PEEM imaging experiment well, which proved that the constructive interference between incident light and scattered light in the slit resulting in the increase of coupling efficiency, as shown in Fig. 5(c). In addition, they analyzed the backward scattering SPP signals and the dependency of EM field distribution through and inside the slit, which were difficult to detect experimentally. The relevant results have certain guiding significance for dynamic controlling of femtosecond SPP.

Besides nano-slits and gratings, nanowires can also be used as ultrafast SPP waveguides.^[56] In 2011, Rewitz *et al.* investigated the propagation characteristics of ultrafast SPP pulses in an Ag nanowire by far-field spectrum interferometry.^[57] They irradiated one end of the Ag nanowire with linearly polarized femtosecond laser pulses (800-nm wavelength) to excite SPP pulses. The excited SPP pulses propagated along the nanowire at a certain group velocity V_g , then re-emitted into free space at the other end of the nanowire (Fig. 5(d)). Afterwards, the author obtained the amplitude and phase of the emission field by collinearly superposing the re-emitted signal with the reference pulse at a fixed time delay time τ with the method of spectrum interferometry, so as to study the propagation characteristics and the change laws of group velocity of femtosecond SPP in Ag nanowire. They found a sharp decrease of the SPP group velocity in the nanowire with diameter lower than 100 nm, as well as smaller dispersion in the propagation process. Besides, they also studied the dependency of ultrashort SPP group velocity on the environment around nanowire. This method can be used to determine the complete spectrum transfer function, and has important application prospects in nanoscale SPP signal characterization and on-chip light signal manipulation.

When a nanodot is fabricated on a metal film, the LSP can be effectively excited through its interaction with incident light. Based on this idea, Lemke *et al.* designed a structure consisting of an Au step and an Au nanodot (500 nm in diameter) on a silicon substrate, and studied the ultrafast interference and transformation process between LSP and SPP excited under the effect of femtosecond laser pulses in 2011.^[58] They applied femtosecond laser (815 nm, 18 fs) to irradiate the Au step at an incident angle of 65 °C to excite SPP pulses propagated along the Au film/air interface. The SPP pulse interacts with the Au nanodot to form LSP mode, and then propagating further away in the form of SPP pulse. After imaging the process with an interferometric time-resolved two-photon photoelec-

tron emission microscopy (ITR-2PPEEM), they achieved the ultrafast process of interference and transformation between the propagated SPP and LSP with sub-femtosecond temporal resolution, as shown in Fig. 5(e). This method provides a new way for direct quantitative analysis of SPP pulse propagation, SPP-LSP coupling, coherent control over LSP excitation at the nanodot, etc. Similarly, in 2013, Sun *et al.* studied the ultrafast oscillation and dephasing process of LSP field excited on Au nanodot arrays with a multi-photon photoelectron emission microscopy (MP-PEEM) system.^[59] LSP can be excited effectively when its wavelengths overlap with the femtosecond pulse spectrum, leading to multi-photon photoelectron emission. The PEEM system with 8 nm spatial resolution was used to directly image the local field excited on different Au nanodots, so as to accurately capture the near-field images, position of local enhancement hotspots and polarization distribution. In addition, the author researched the LSP characteristics by combining the interferometric time-resolved pump-probe technology with PEEM, and achieved the ultrafast oscillation and dephasing process of LSP field with femtosecond-scale temporal resolution and nanoscale spatial resolution, as shown in Fig. 5(f). This method provides an effective access to research on near-field imaging and dynamic characteristics of SPP nanostructures.

Besides the nanostructures fabricated on metal film, a thin metal film with specific shape can also be used to effectively excite femtosecond SPP. In 2017, Frank *et al.* designed the atomic-scale flat hexagonal mono-crystal Au film and studied the propagation process of short-range SPP pulses excited on its surface.^[60] The sharp edges of the Au film provided necessary wave vector compensation for SPP excitation. Stimulated by femtosecond laser pulses (800 nm, 15 fs, and 80 MHz), the long-range femtosecond SPP pulse (LR-SPP) and short-range femtosecond SPP pulse (SR-SPP) were excited on the upper and lower surfaces of the Au film at the edge, respectively. Then the time-resolved 2PPE-PEEM system was used for imaging the excited SPP waves. The author found that LR-SPP could propagate on the whole Au film surface while SR-SPP could propagate within a range of several wavelengths from the edge. Then they designed a triangular Au film with a periodic circular grating and a concentric disc (2- μ m diameter), and investigated the ultrafast nanofocusing process of excited SR-SPP with the combination of pump-probe technology and PEEM system. SR-SPP was excited at the circular grating, then propagated toward the center of the disc. Finally, a near-field focus with minimum spatial size of 60 nm was formed through the superposition of SPP waves. Due to the constructive and destructive interference of the laser field and the two counter-propagation SPP waves, the SPP intensity of the focus changed periodically, as shown in Fig. 5(g). This method provides a new idea for nanofocused SPP generation and local field enhancement.

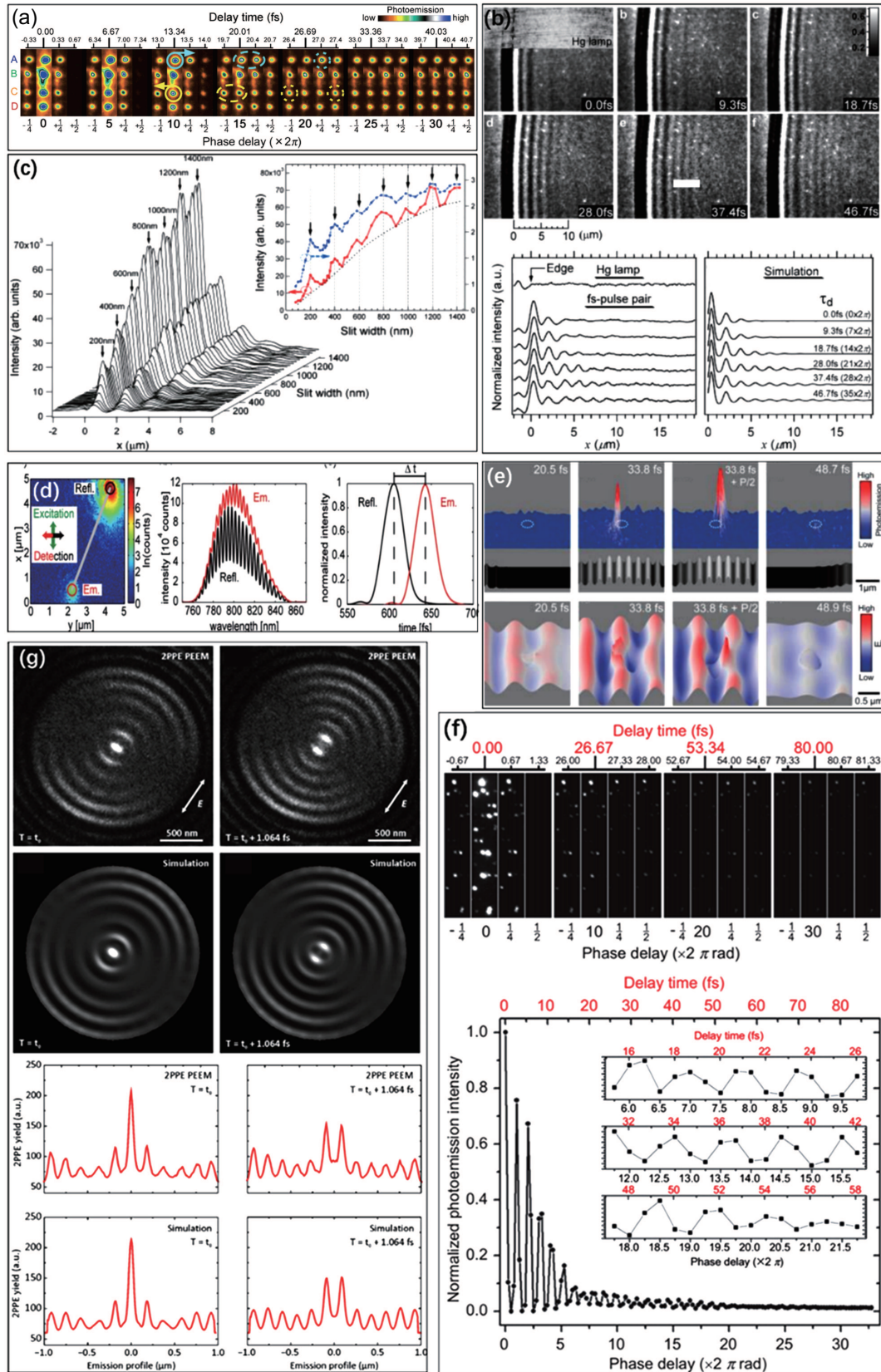


Fig. 5. (a) ITR-PEEM of the four localized plasmons on the Ag grating framed.^[50] The delay time between the pump and probe pulses (τ_d) is advanced from -0.33 fs to 40.69 fs or $-\frac{1}{4} \times 2\pi$ to $30\frac{1}{2} \times 2\pi$ in terms of the optical phase of the carrier light (400 nm) with an increment step of 0.33 fs or $\frac{1}{2}\pi$. All four dots oscillate in-phase with the field during the optical excitation by the pump pulse ($-\frac{1}{4} \times 2\pi$ to $30\frac{1}{2} \times 2\pi$). (b) ITR-PEEM movie frames of the Ag film excited with phase-locked pump-probe pulse pairs.^[54] (c) Slit width dependence of the polarization grating pattern.^[55] (d) Representative map of sample emission upon excitation of plasmons in an Ag nanowire.^[57] (e) Au step and Au nanodot excitation via SPP coupling recorded in real time.^[58] (f) Selected TR-MP-PEEM images at different phase delays/delay times for an array of Au nanorods.^[59] (g) PEEM detection and simulation results of the SR-SPP nanofocus process.^[60]

3.2. Excitation and focusing characteristics of femtosecond SPP at metal nanoprobe

The conical metal nanoprobe has the property that the closer it is to the apex, the smaller its lateral size, which is similar to a focusing process. If a grating was etched on a nanoprobe, laser energy can be effectively coupled to SPP under the excitation of femtosecond laser pulses, and the ex-

cited SPP wave could propagate along the surface toward the apex. During the propagation process, as the cross-sectional size of the nanoprobe gradually decreases, the local field becomes stronger and stronger, resulting in significant EM field enhancement at the apex. When the field intensity is strong enough, high-order nonlinear effect and HHG could occur at the apex.

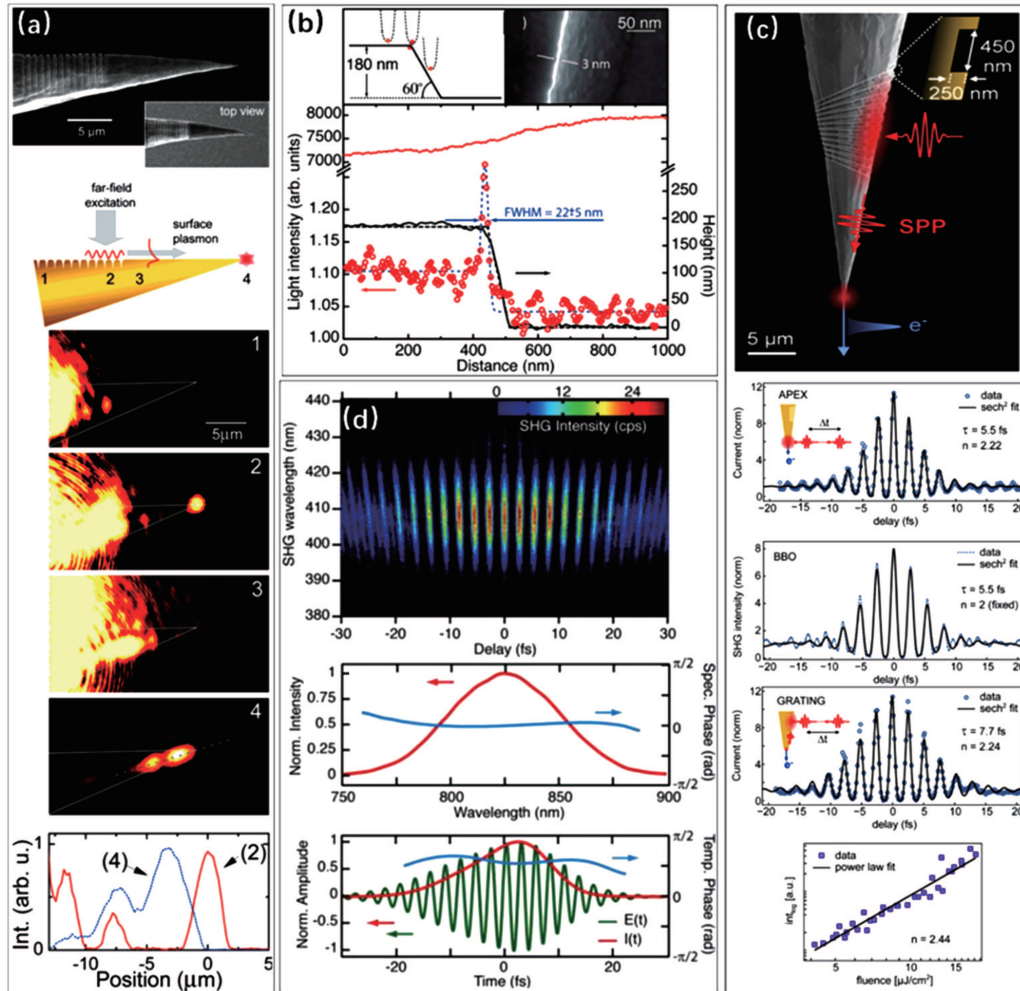


Fig. 6. (a) SEM images of a conical metallic tip with a grating coupler on the shaft, principle of the nonlocal excitation of the tip apex and series of microscope images recorded for illumination of the tip at the four positions.^[61] (b) Schematic diagram of scanning the nanofocusing tip across a silicon step edge, SEM image of step edge, and the optical signal of a lateral scan across the step edge.^[62] (c) SEM image of an Au tip with a chirp grating coupler 20 μm away from the apex.^[63] (d) Nanofocusing of a few femtosecond pulse at the tip: FROG measurement based on apex localized SHG of adiabatically nanofocused SPP, and reconstructed spectral and temporal phase (blue), intensity (red), as well as the reconstructed temporal electric field transient (green).^[64]

In 2007, Ropers *et al.* achieved the nanoscale focusing plasmonic field that exceeded the diffraction limit by utilizing the nanofocusing characteristics of the conical Au nanoprobe.^[61] The author designed a tapered Au nanoprobe (with an apex angle of 15°) etched with one-dimensional (1D) circular grating (10 μm away from the apex, with a radius of 20 nm. SEM image shown in Fig. 6(a)), and used it as the SPP excitation coupler. Broadband femtosecond laser pulse (800 nm, 7 fs) was normally entered and focused at the coupler (the diameter of focus was about 5 μm) to excite SPP pulses. The imaging of far field radiation at the apex was captured

by scanning tunneling microscope (STM). They found that micron-scale femtosecond laser pulses can be transformed into nanoscale SPP pulses with the coupler, which provided to be a useful tool to generate nanoscale light sources. Based on this, in 2010, Neacsu *et al.* experimentally obtained the focused femtosecond SPP pulses localized at the scale of 20 nm,^[62] whose spatial size was an order of magnitude smaller than the diffraction limit (Fig. 6(b)). In 2016, Müller *et al.* excited the ultra-broadband femtosecond SPP through chirped grating coupling etched on an Au nanoprobe, and achieved a nanofocus at the apex,^[63] as well as a sub-10-fs electronic pulse point

source there, as shown in Fig. 6(c). These works provide new methods for investigating new type of field enhancement microscopes, HHG or attosecond extreme ultraviolet (EUV) laser generation, and ultrafast STM, *etc.*

Chirped grating can be used as a broadband-spectrum ultrashort SPP pulse coupler as its capacity of broadband coupling ability. With this method, Berweger *et al.* achieved the generation and controlling of ultrashort pulses with arbitrary optical waveform by a conical Au nanoprobe etched with a chirped grating in 2011.^[64] The nanoprobe was irradiated by focused femtosecond laser pulses (800 nm, 10 fs, 8 nJ/pulse, and 75 MHz) to generate broadband-spectrum SPP pulses. The excited SPP pulses were compressed and propagated toward the apex of the nanoprobe, causing a few SPP pulses being re-emitted into free space. In addition, the asymmetry of the apex allowed local second harmonic generation (SHG).^[65] The instantaneous frequency and spectral phase of femtosecond pulses can be optimized by taking the SHG response as the feedback signal of pulse shaping mechanism, so as to generate, regulate and control arbitrary independent nanoscale ultrafast optical waveforms at the apex (Fig. 6(d)). Compared with traditional far-field and near-field light sources, this nanoscale light source with controllable waveform is of great significance, which provides a new solution of super spatiotemporal imaging for multiform nonlinear and ultrafast processes.

3.3. Spin-orbital angular momentum interaction characteristics of femtosecond SPP

As is known that photon can carry both spin angular momentum (SAM) and orbital angular momentum (OAM), and

the SAM–OAM conversion can be achieved with some special structures. The subwavelength-scale SPP also have the ability of carrying OAM. For example, it has been proved that the Archimedean spiral and relevant nanostructures can be used to generate and control the SPP vortex with OAM under different lighting conditions.

Therefore, the highly localized SPP vortex can be regarded as an important tool for researching chiral nanostructures and two-dimensional (2D) materials with degree of freedom of OAM.^[66] In order to characterize the formation process of SPP vortex field carrying OAM, in 2017, Spektor *et al.* excited the SPP vortex field by a nanoscale metal structure irradiated with femtosecond laser pulse, and achieved the ultrafast temporal evolution process and group velocity characteristics of SPP vortex generation.^[67] A circular polarization femtosecond laser pulse is used to illuminate the Archimedes spiral slit etched on an Au film. The edge scattering effect of the slit provided necessary wave vector compensation to excite SPP propagating towards the center at the interface, and the spiral shape of slit provided helical phase for the excited SPP. The SAM–OAM conversion could occur under circular polarized light illumination. Therefore, the OAM of generated SPP vortex was finally determined by the helical phase provided by the slit and the SAM carried by incident photons. The ultrafast evolution process of SPP vortex field with topological charge of 10 in a single optical period (~ 2.67 fs) was studied by means of pump-probe detection, as shown in Fig. 7. This is of great significance in further understanding the generation and evolution characteristics of OAM and its dynamic interactive process with atomic and molecular.

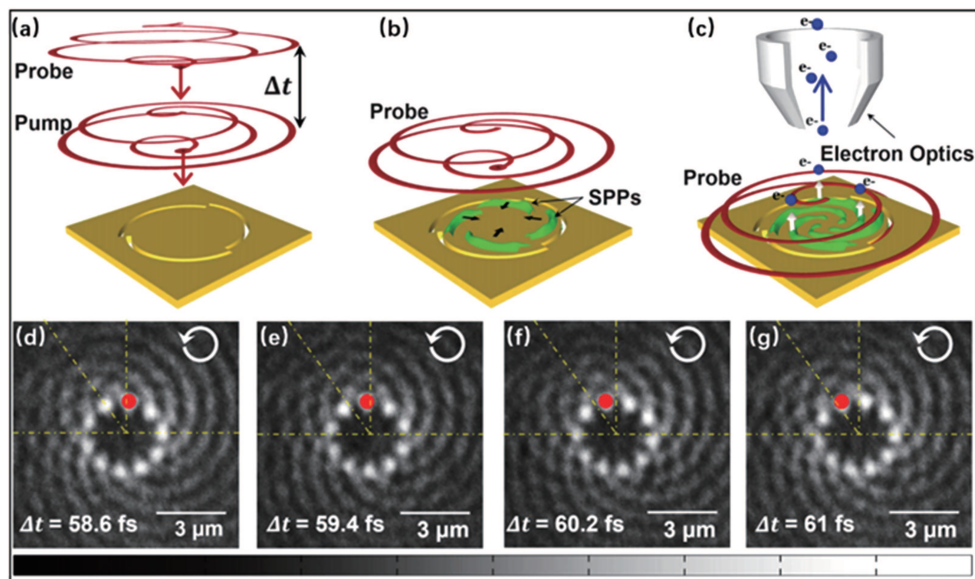


Fig. 7. Experimental concept and direct OAM extraction results.^[67] (a)–(c) Schematic experimental methodology. (a) Two circularly polarized ultrashort pulses with temporal separation Δt are launched at a plasmonic vortex-generating sample. (b) The pump pulse launches SPPs at the structure edges on the sample. (c) The probe pulse interferes with the propagating SPPs and liberates photoelectrons in a 2PP process, which are then imaged with the PEEM setup. (d)–(g) Experimental TR-PEEM snapshot sequence of the rotating field of a plasmonic vortex in the revolution stage within a single optical cycle of ~ 2.67 fs. The red dot follows a specific lobe as it rotates around the center. The yellow dashed-dotted lines serve as reference frames to emphasize the rotation. The angle between the upper two yellow lines is 36° , corresponding to $2\pi/10$ rads.

4. Research progress on applications of femtosecond SPP

Femtosecond SPP has been widely applied in detecting ultrafast phenomena including molecular dynamics, biomedicine, SRS and photoelectronic chips for its unique properties. Its common applications cover the fields of nonlinear optical enhancement, optical tweezers, on-chip photonic manipulation, super-spatiotemporal imaging and pulse shaping. In the following, we will introduce and analyze some important application researches of femtosecond SPP in recent years.

4.1. Nonlinear signal enhancement by femtosecond SPP

SPP can be used to effectively enhance nonlinear optical response due to its unique characteristics of local EM field enhancement.^[15,68] If femtosecond laser pulses and SPP were combined, the high-order nonlinear optical effects of materials can be easily excited owing to the ultrahigh peak power and local EM field enhancement effect of femtosecond SPP pulses,

thus resulting in a significantly enhanced nonlinear effect and greatly improving nonlinear conversion efficiency. Thus, femtosecond SPP has widespread application prospects in some fields such as EUV source and nonlinear signal enhancement, as its remarkable high order nonlinear effect and high nonlinear conversion efficiency.

In 2008, Kim *et al.* obtained EUV pulses by focusing femtosecond laser pulse (800 nm, 10 fs, 75 MHz, 1.3 nJ/pulse, 10^{11} W·cm⁻²) onto a bowtie-shaped metal nanostructure.^[5] The bowtie structure can excite LSP mode to form a Gap mode enhancement in the middle of the bowtie, and produce high-order nonlinear effect under the action of nitrogen flow, so as to realize HHG. With this structure, the author obtained 17th order harmonics (47 nm) with the corresponding conversion efficiency of 6.9×10^{-10} , as shown in Fig. 8(a). This method is useful in generating ultra-small coherent EUV radiation sources, and facilitates the development of advanced photoetching, high resolution imaging, EUV measurement and other areas.

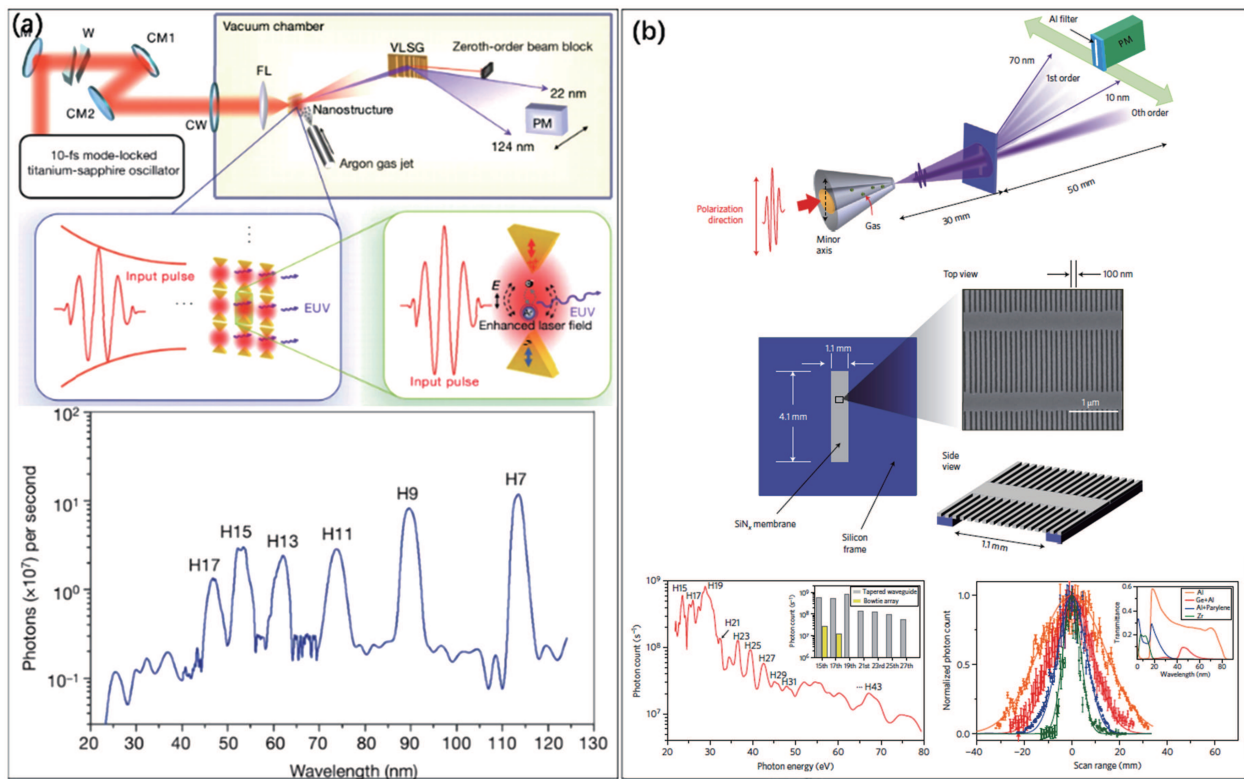


Fig. 8. (a) Apparatus for HHG by electric field enhancement using a nanostructure of bowtie elements and measured spectrum of generated high harmonics.^[5] Given the input pulse power of 100 mW, the efficiencies for the harmonics were computed as follows: H7, 2.4×10^{-9} ; H9, 2.2×10^{-9} ; H11, 9.5×10^{-10} ; H13, 9.0×10^{-10} ; H15, 1.3×10^{-9} ; and H17, 6.9×10^{-10} . (b) Measurement scheme using a transmission-type diffraction grating and a photomultiplier (PM) tube, SEM images of the grating showing the important dimensions and measured spectrum spanning from the 15th (H15) to 43rd (H43) harmonics.^[41]

In 2011, Park *et al.* designed a three-dimensional (3D) Ag nanoscale waveguide to achieve high-order EUV pulses.^[41] The waveguide had an elliptic conical hole at its center. The cross section of the elliptic hole gradually decreases from the entrance (short diameter 2 mm) to the exit (short diameter 100 nm). Femtosecond laser pulses (800 nm, 10 fs,

75 MHz, 1×10^{11} W·cm⁻²) were focused on the inlet of the waveguide and propagated along the outlet through the hole. Through adiabatic compression of the 3D waveguide, the incident femtosecond laser pulses were focused into the deep subwavelength volume at the exit, resulting in a significant increase of the electric field intensity, with EF over 20 dB

and reaching the ionization threshold of xenon. Thus EUV pulses were generated by femtosecond laser pulses interacting with xenon atoms. The author obtained the 15th to 43th order higher harmonic EUV pulses with high spatiotemporal coherence (Fig. 8(b)), and the nonlinear conversion rate reached 10^{-8} . Compared with bowtie-shaped structure mentioned previously, this waveguide effectively improved the conversion efficiency without considering thermal damage and optical breakdown. Additionally, this waveguide can be easily inserted into the cantilever nanoprobe, which makes it more suitable in near-field optical experiments.

Except high-order EUV pulses generation, the nonlinear signal enhancement effect of femtosecond SPP pulse is also one of the hot researching topics. In 2003, Nahata *et al.* designed a bull's-eye structure consisting of periodical concentric circular grooves and a nanohole based for the enhanced nonlinear optical characteristics.^[69] Compared with a single

nanohole, this designing increased the SHG conversion efficiency by four orders of magnitude, as shown in Fig. 9(a). In 2010, Pu *et al.* investigated the nonlinear enhancement characteristics of SPP nanocavity of core-shell (BaTiO₃-Au) structure under different resonant conditions,^[70] as shown in Fig. 9(b), the SH enhancement results of 500 times and 3500 times were obtained by experiment and simulation respectively. Subsequently in 2011, Zhang *et al.* studied the relationship between the orientation of metal sphere-cap NPs and the included angle of femtosecond laser pulses to SH radiation intensity,^[71] and paved the way for designing of stable second-order nonlinear optical materials with specified wavelengths. In 2012, Hanke *et al.* found that the geometry of the nano-antennae will greatly affect the radiation damping of its LSP resonance,^[72] thus determining the generation efficiency of the third-order harmonic.

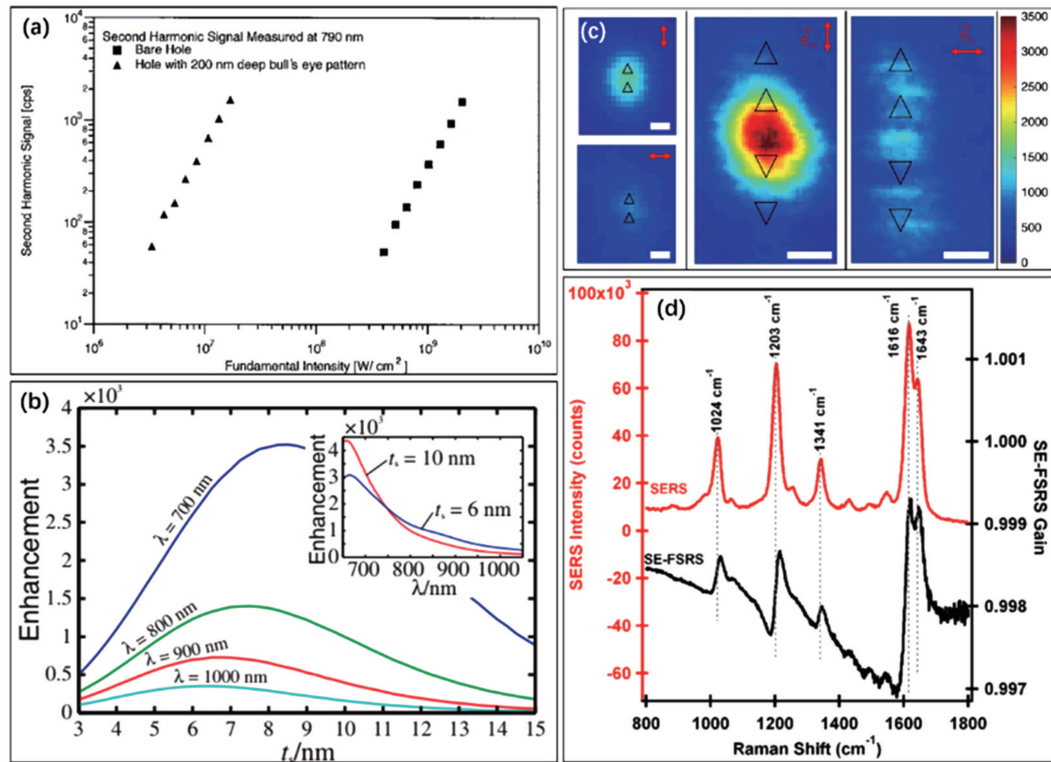


Fig. 9. (a) SH intensity dependence versus fundamental intensity for both the bull's-eye structure and the bare aperture.^[69] (b) Factor of SHG emission enhancement as a function of the shell thickness for different resonance frequencies.^[70] (c) SHG from a flat centrosymmetric triangular nanocavity on Ag film.^[73] (d) SERS spectrum and SE-FSRS spectrum of trans-1, 2-bis(4-pyridyl) ethylene (BPE)-functionalized nanoantennas.^[74]

Besides complex structures mentioned above, the nanocavity on smooth Ag film has also been proved to be a useful tool for SH radiation enhancement.^[73] In 2018, Galanty *et al.* designed two pairs antisymmetric distributed triangular nanocavities structures, as triangular nanocavities has the characteristics of supporting multiple SPP modes. The structures could localize the EM field on the smooth surface between nanocavities and modulate the resonant frequency by adjusting the distance between two nanocavities. By observing the SH radiation responses of the structure, the author found that the

SH radiation enhancement only occurred in the area between two sub-cells, when the polarization of incident femtosecond laser field was along the symmetry axis of the structure, while the SH radiation intensity sharply decreased as the polarization direction was rotated by 90 °C, as shown in Fig. 9(c). Based on the calculations, the author concluded that the existence of the nanocavities increases the SH radiation on the Ag film by 7 times, proving that the nanocavities played a key role in SH radiation enhancement. The work demonstrated a new idea for generating SH hotspots at any given positions on a metal

surface. In addition, this locally enhanced SH hotspots provide a useful tool for researching the physical and chemical processes occurring on the surface.

Considering the ultrahigh nonlinear signal enhancement ability of femtosecond SPP, it would be a promising approach to achieve highly sensitive Raman spectrum signal detection when it was combined with Raman spectrum study. Based on this idea, in 2011, Frontiera *et al.* put forward surface-enhanced femtosecond stimulated Raman spectrum (SE-FSRS) technique by combining SERS technology with femtosecond stimulated Raman spectrum (FSRS) technology,^[74] and they investigated the stimulated Raman enhancement effect of the Au nano-antenna consisting of an Au core, inserted molecules and a silicon dioxide shell under the irradiation of femtosecond laser pulses. Then compared SE-FSR spectrum intensity (black) of Au NPs with SERS spectrum intensity, as shown in Fig. 9(d), they found that the EF of SE-FSRS spectrum was between 10^4 and 10^6 , less than 10^8 in the SERS enhancement experiment of the NPs. They suggested that this difference was due to NPs degradation. Besides, the SE-FSR spectrum was obtained with signal to noise ratio (SNR) of 50, as well as high spectrum resolution (20 cm^{-1}) and high temporal resolution (10 fs–100 fs), which proved that SE-FSRS technology could be applied in the detection of NPs. These works show that femtosecond SPP pulses can be used to generate high harmonics and to improve multiple nonlinear signals and nonlinear conversion efficiency by designing appropriate plasmonic nano-structures.

4.2. Optical tweezers of femtosecond SPP

SPP optical tweezers technology is an important technical means for near-field capturing and accurate manipulation of micro-/nano-particles. The basic mechanism is to use nano-structures to excite SPP and form local enhancement hotspots much smaller than the diffraction limit, so as to provide super-intense gradient force for capture and nanoscale manipulation precision. Femtosecond SPP not only has local enhancement effect of SPP, but also has ultrahigh peak power of femtosecond pulse. If it was applied to optical tweezers, it may not only further enhance the optical trapping force and trap stability of NPs, but also can greatly enhance the nonlinear effect of trapped samples to generate more novel physical phenomena.

The precondition for generating femtosecond SPP optical tweezer is to design a proper optical tweezer structure that can create SPP hotspots. Guided by this principle, Roxworthy *et al.* designed an optical tweezer structure based on a bowtie-shaped Au nano-antenna array in 2012.^[75] A femtosecond SPP optical tweezer was obtained by combining the designed structure with femtosecond laser pulse. An inverted microscope system was utilized to study the enhancement effect of the femtosecond SPP optical tweezer on optical gradient force,

and a higher optical tweezer trapping efficiency was achieved. The optical trapping potential was twice or five times as much as that of the continuous wave optical tweezers or the traditional pulsed optical tweezers, respectively. Such femtosecond nano-optical tweezers could not only successfully capture Ag NPs with diameter of 80 nm, but also could detect the nonlinear response of NPs system, as shown in Fig. 10(a). In 2016, Kotsifaki *et al.* also realized the femtosecond SPP optical tweezers by using femtosecond laser incident on nanostructure silicon substrate.^[76] The substrate consists of a thin Au film with Au NPs on its surface. A thin copper interlayer was introduced to effectively transfer heat to avoid the generation of bubbles. Continuous infrared laser or femtosecond laser with adjustable wavelengths (750 nm–1300 nm) was used for optical trapping. The author observed a significant increasing of trapping efficiency for polystyrene beads with diameter of 400 nm near the substrate, and the maximum trapping efficiency was 0.147. By measuring the optical trapping force and distance from the substrate, it was found that the trapping efficiency decreased exponentially as the distance increased, which confirmed that the trapping process was dominated by the evanescent field. Furthermore, when the incident wavelength approached SPP resonant wavelength of substrate, the trapping efficiency increased accordingly, as shown in Fig. 10(b).

Affected by the ultrahigh peak power of femtosecond laser pulses, as well as LSP of NPs, the nonlinear optical effect of metal NPs was greatly enhanced, showing unusual nonlinear trapping effects of optical tweezers. In 2010, Jiang *et al.* reported that the ‘light trapping splitting’ phenomenon appeared when an intense linearly polarized femtosecond laser was focused to trap Au NPs,^[42] that is, with the nonlinear interaction between femtosecond laser pulses and Au NPs, the optical trapping that could trap only a single NP under continuous laser irradiation could be split into two, and would trap two NPs at the same time (Fig. 10(c)), which revealed the prospects of optical tweezers manipulation under nonlinear conditions. Based on this, in 2018, Zhang *et al.* further studied the physical mechanism of such nonlinear effect between light fields of focused femtosecond laser pulses and metal NPs,^[43] and achieved tunable multiple trapping of Au NPs by using femtosecond laser pulses with vector polarizations. Unlike the mechanical effect in a linear condition, the longitudinal electric field component of the focused femtosecond light field played a dominant role and established a new force balance, so as to create multiple trapping potentials at the focus of the longitudinal component (Fig. 10(d)), and realized stable multiple traps of NPs. This work laid a foundation for the research of optical tweezer technology from linear optics to nonlinear optics and generating more nonlinear optical manipulation technologies.

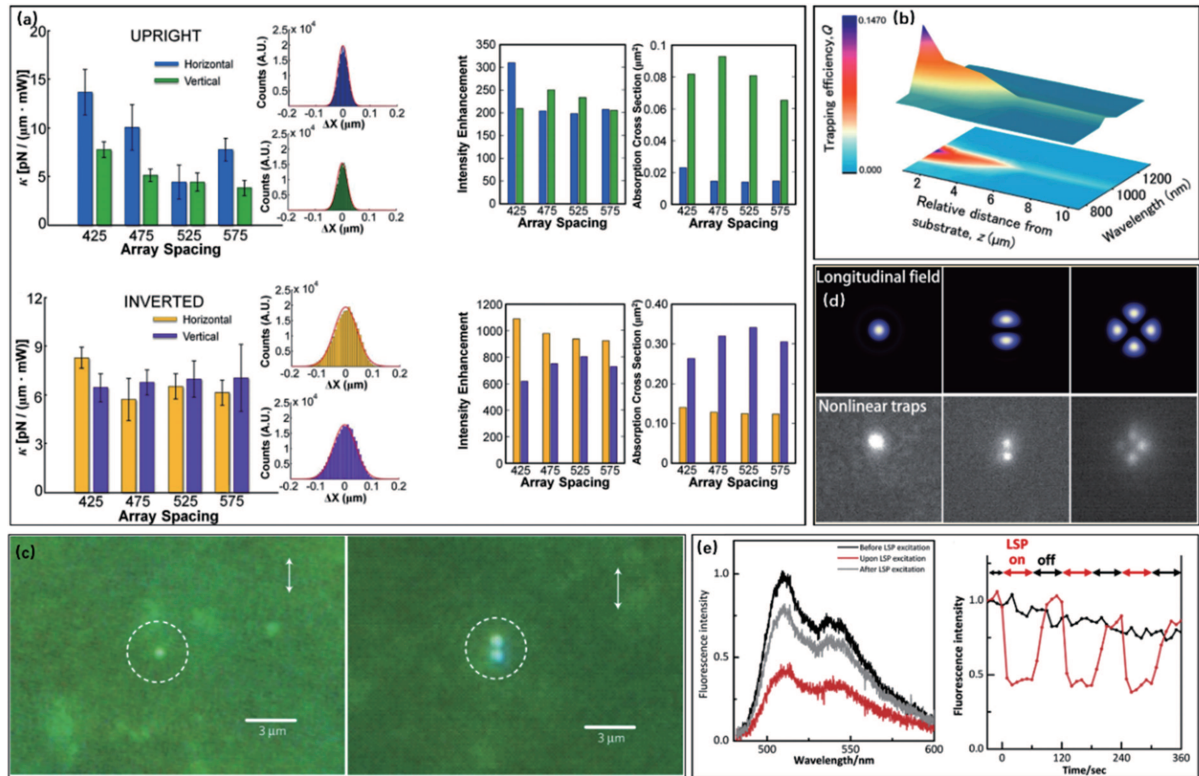


Fig. 10. (a) Experimentally measured trap stiffness for the upright BNA orientation and the inverted BNA orientation, and FDTD calculations of the intensity enhancement and absorption cross-section for the upright BNA orientation and the inverted orientation.^[75] (b) Surface plot of the trapping efficiency, Q , as a function of the relative distance, z , between the trapping laser beam focus and the Cu/Au-coated nanostructured silicon substrate and as a function of the trapping wavelength, obtained with the femtosecond laser setup.^[76] (c) Au NPs trapped by the Ti-sapphire laser in the CW mode (left) and femtosecond pulse mode (right). White arrows show the directions of polarization.^[42] (d) Nonlinear trapping of Au NPs under various polarization conditions.^[43] (e) DNA assembly on a thin Au film with no nanostructure using femtosecond NIR laser irradiation.^[77] (left) Fluorescence spectra obtained before (black), upon (red), and after (gray) femtosecond laser irradiation. (right) Temporal profiles of the fluorescence intensity as the laser was switched on and off repetitively (red, repetition time ≈ 60 s) and without femtosecond laser irradiation (black).

One of the important application objectives in nanoscale optical tweezers research is to trap and manipulate biological molecules such as DNA. In 2013, Shoji *et al.* studied the trapping behaviors of LSP optical tweezers excited on taper-shaped Au nano-dimer array under continuous light and NIR femtosecond laser pulses illumination,^[77] respectively. They achieved permanent fixation, tunable trap and release of λ -DNA molecules. The trapping behavior of LSP optical tweezers was observed by fluorescence microscopy, and the temperature variation of LSP excitation was evaluated by fluorescence correlation spectrum. As shown in Fig. 10(e), when LSP was illuminated with continuous light, the fluorescence intensity did not change significantly over time, while irradiated by a femtosecond laser pulses, the fluorescence intensity fluctuated periodically as the laser pulses were switched on or off. The author concluded that the former was due to photothermal effect induced by LSP excitation, which leads to permanent fixation of DNA molecules on the substrate, and the latter was attributed to the great gradient force of femtosecond laser pulses to overcome the thermophoresis effect, and the existence of the pulse interval prevented DNA molecules from being fixed on the substrate. Therefore, any desired micropatterns of DNA molecules can be formed on the substrate by photothermal effect induced by LSP excitation, and DNA

molecules can also be dynamically controllable captured and released by turning on and off of femtosecond laser irradiation. This femtosecond LSP optical tweezers technology provides an effective access for manipulation of nucleic acid, protein, polysaccharide and other small biomolecules, and thus has important potential applications in the fields of chemical, biological sensing and detection.

4.3. On-chip modulation of femtosecond SPP

For its characteristic of breaking diffraction limit, SPP has been widely applied in many micro-/nanoscale on-chips optical devices, including optical waveguide, switches and modulators, *etc.* Similarly, femtosecond SPP may bring new ideas to on-chip spatiotemporal light field manipulation. In 2018, Hess *et al.* studied on-chip beam splitting and polarization multiplexing of femtosecond SPP waves.^[78] They designed an Ag hemispherical structure (9 microns in diameter and 940 nm in height) and demonstrated that it can scatter s-polarized femtosecond laser pulses and excite femtosecond SPP, then coupling the femtosecond SPP into two separate channels in space and time, resulting in pulse-splitting effect. In their structure, SPP was generated by scattering of the hemispherical structure under the illumination of femtosecond laser pumped pulse (780 nm, 15 fs, incident angle of 75°). The probe pulse ir-

radiated on the SPP propagation region, meanwhile interfered with the SPP pulse, led to an SPP interference pattern. They found that the SPP interference patterns obtained from pump–probe pulse combination by using the p–p or s–p polarization were crescent shape and staggered herringbone-shape, respectively, as shown in Figs. 11(b)–11(c). With the s–p polarized pump–probe pulse combination, two anti-symmetrical interference field patterns in time response on the upper and lower planes

were obtained by changing the relative delaying time with half optical cycle (1.24 fs), as shown in Figs. 11(d)–11(e), suggesting that the generated femtosecond SPP could propagate in the upper and lower planes at different times. This work opens up a new idea for researching on on-chip manipulation of femtosecond SPP such as polarization multiplexing and pulse splitting, *etc.*

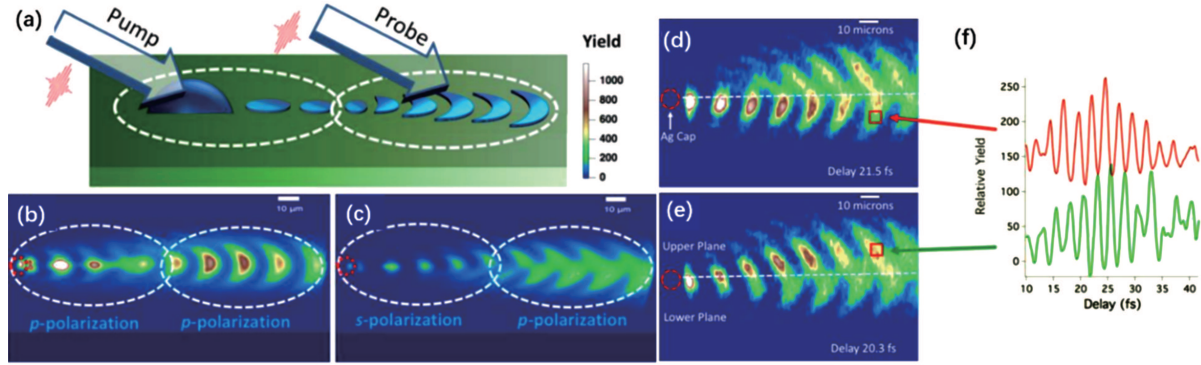


Fig. 11. (a) Schematic illustration of the spatially separated pump–probe experiment. (b) PEEM image following excitation with 780-nm p-polarized spatially separated femtosecond pulse pairs. (c) PEEM image of the same hemisphere but recorded following excitation with s-polarized laser pulses and probed using p-polarized pulses. Red dashed circles mark the location of the hemisphere and white dashed ovals indicate the approximate positions of the spatially separated pump and probe beams. (d) PEEM images following excitation with 780-nm s-polarized femtosecond pump pulses and p-polarized probe pulses separated by approximately one-half period (1.24 fs). (f) Time trace of electron yield from the red boxed areas in panels (d) and (e) as a function of relative delay between the pulses. The resulting trace demonstrates that the SPP in the upper plane is π radians out-of-phase with that generated in the lower plane.^[78]

4.4. High spatiotemporal resolution imaging of femtosecond SPP

Due to the combination of ultrashort laser pulse and SPP, femtosecond SPP both have excellent features of femtosecond-scale temporal resolution and nanoscale spatial resolution in theory, which makes it more suitable for observing ultrafast interaction processes between light and matter in an extremely small spatiotemporal scale that cannot be detected by conventional methods, including molecular dynamics, ultrafast photosynthesis process and molecules SRS, *etc.* Therefore, femtosecond SPP imaging technology has immeasurable potential values in fields such as biomedicine and nanophotonics.

In 2015, Mittal *et al.* measured the ultrafast emission process of femtosecond LSP excited on a single Ag NP or cluster.^[79] They used pump–probe femtosecond pulses to irradiate the Ag NP on the total internal reflection structure, and then measured the LSP coherence spectrums excited by the two laser pulses. Different frequency components and dephasing rate of each NP was obtained by Fourier transform analysis on the nano-plasmonic coherence oscillation, and three different types of behaviors appeared, including single exponential decay, beat between two frequencies and beat among multiple frequencies. A pair of NPs were shown in Fig. 12(a). It can be seen that their LSP coherence were in-phase at $\tau = 0, 38$, and 75 fs, while out of phase at $\tau = 22$ and 54 fs, as a result of their difference in frequency. The ultrafast dynamic process can be monitored in real time, and the non-uniform and uniform spec-

trum broadening with LSP can be measured by individual NPs detection. The method greatly expanded the application of Ag NPs in biological sensing, solar energy trapping and other fields.

In 2016, Kravtsov *et al.* achieved nonlinear four-wave mixing (FWM) effect and femtosecond SPP nanofocusing phenomenon by coupling ultrashort laser pulses with a grating etched on an Au nanoprobe.^[40] The ultrafast nanoscale imaging of femtosecond SPP coherent dynamic process at different hotspots on the rough Au film was captured, as shown in Fig. 12(b). The incident femtosecond laser pulses were coupled by the grating to generate ultrashort SPP pulses that propagate toward the apex of the nanoprobe. The propagated SPP was dramatically amplified by the asymmetric adiabatic compression effect of the nanoprobe, and then focused on the apex, resulting in the formation of a highly-localized enhanced light field. Hence nonlinear FWM effect taken place, and directly lead to far-field radiation of third-order nonlinear signal with the nonlinear conversion efficiency up to 1×10^{-5} . Subsequently, they imaged a rough Au film with this nonlinear nanoprobe, and achieved the few-femtosecond coherent dynamics process of plasmonic hotspots with 50-nm spatial resolution and 8.2-fs temporal resolution. This work shows a new design scheme of high sensitive nanoprobe for ultrafast near-field microscope and spectroscopy research, and may have great application in coherent, ultrafast, multi-dimensional and all-optical near-field spectral imaging.

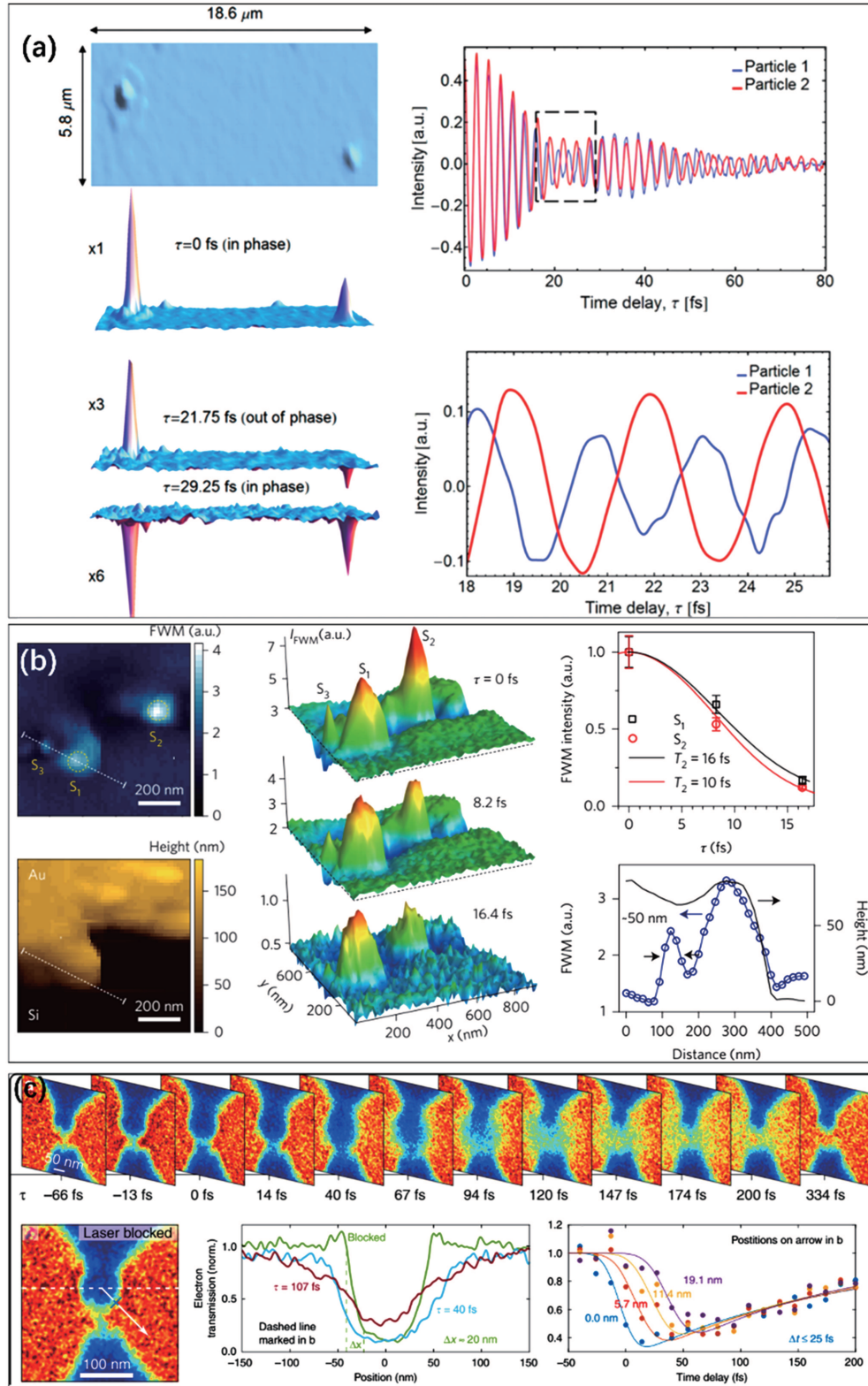


Fig. 12. (a) 3D intensity plot of two particles (1, 2) at time delays: $\tau = 0, 21.75$, and 29.5 fs (left) and comparison of the plasmon signal from the two NPs (right).^[79] (b) Femtosecond FWM nanoimaging of coherent plasmon dynamics in Au film.^[40] (c) Dynamics of photoemission from the gap of a single plasmonic nanoantenna.^[80]

To observe electronic motion in nanoscale and femtosecond-scale is one of the most important goals for modern ultrafast science. In 2018, Vogelsang *et al.* combined ultrafast-projection electronic microscope (UPEM) with pump-probe technology to study the ultrafast photoelectronic emission pro-

cess on a conical Au nanoprobe,^[80] and achieved ultrafast spatiotemporal motion process of emitted electrons with 20-nm spatial resolution and 25-fs temporal resolution. They used the conical Au nanoprobe to focus femtosecond SPP pulses on the apex, forming a nanoscale light source that radiated ultra-

short electronic pulses with a pulse duration less than 10 fs. The electron pulse was used as the probe source, after being diffracted by a plasmonic nano-resonator (two holes with a diameter of 400-nm etched on a 30-nm Au film and connected by a 30-nm slits), the ultrafast motion trajectory of radiated electron was tracked and recorded by the UPEM system. They found that the UPEM image shows an evenly distributed transmissivity of probe electrons in the transparent area of the nano-resonator with no pump pulses irradiation, while a sharply decrease of electronic transmittance around the slit appeared with a certain time delay between pump and probe pulses. This was because the relatively low velocity of the electrons increases its interaction time with local electric field in the gap area, accordingly resulted in trajectory deflection of probe electronic pulses when passing through low-energy electronic clouds emitted at the gap. Such a spatiotemporal evolution process of electronic cloud could be captured by varying the relative time delay between pump and probe pulses, as shown in Fig. 12(c). This method can be directly used to explore the near-field electronic motion of a single nanostructure, and makes it a useful tool to reveal ultrafast electric charge-carrier dynamics in nanostructures.

4.5. Femtosecond SPP pulse shaping

The propagation of femtosecond SPP pulse is often accompanied by severe dispersion, which limits its application in generating ultrashort pulses. However, the emergence of the femtosecond SPP pulse shaping technology makes up for

this deficiency. According to different needs, this technology can be used to design specific wavefront of incident laser pulse to excite desired SPP pulses with specific time domain waveform, thus providing a novel way to generate ultrashort SPP pulses.

In 2015, Toma *et al.* performed pulse shaping according to the response function of excited femtosecond SPP on a conical Au nanoprobe,^[81] so as to accurately control the waveform of SPP pulses at the apex and generate SH radiation. They adopted an Au nanoprobe etched with circular grating to efficiently couple pump femtosecond laser pulses into SPP pulses. The excited SPP pulses were focused at the apex of nanoprobe and re-emitted to free space. The temporal waveform of re-emitted SPP pulse was obtained by measuring its coherent images with pump pulses as a function of relative delay time. The response functions of propagated SPP on the nanoprobe and re-emitted at the apex were achieved after data processing. According to this response function, SPP pulse shaping at the apex of nanoprobe was realized by using a 4f system to compensate the dispersion of excited pulses. As shown in Fig. 13(a), different SPP spectra could be obtained by altering the wavefronts of incident femtosecond pulses. In addition, the author also successfully dynamically controlled the SH radiation at the apex. This method can be used to generate arbitrarily temporal waveforms of the radiated pulse at the apex, which will expand the application of near-field optical detection systems such as NSOM.

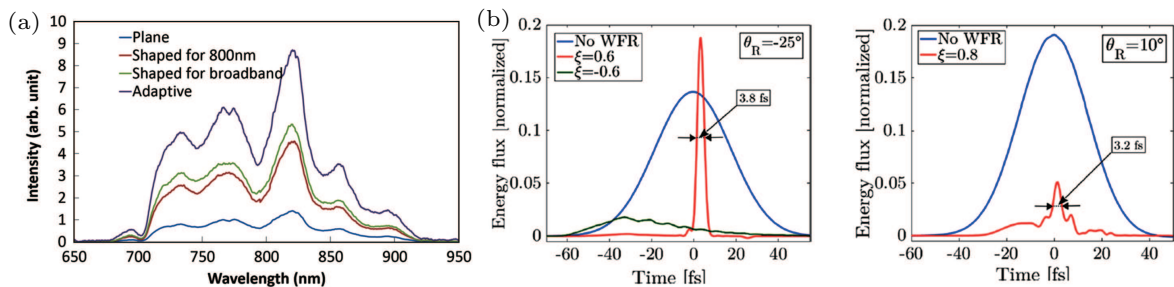


Fig. 13. (a) SPP spectra at apex of tip obtained with various wavefronts incident to the grating fabricated on the tapered Au tip.^[81] (b) Energy fluxes of SPPs generated on a grating by laser pulses incident at different resonant angle θ_R and different WFR velocities ξ .^[82]

In 2018, Pisani *et al.* put forward a method for the generation of few-cycle SPP pulses.^[82] The authors employed femtosecond laser pulses with wavefront rotation (WFR) to irradiate a coupling grating etched on a metal surface. The focus of femtosecond laser pulse rotated in space over time because of WFR. Considering the strict requirement of incident angle for SPP generation, SPP excitation only took place in extremely short time window during WFR process of femtosecond pulse. Therefore, this method can be used to excite SPP in a time window shorter than the duration of incident laser pulse, thus generating ultrashort SPP pulse. Through numerical simulation,

the author found that the incident pulses with central wavelength of 800 nm and duration of 29.5 fs could excite SPP pulses with duration shorter than 4 fs (nearly 1.5 optical cycles), and the peak amplitude of excited SPP pulses was 2.7 times that of the incident pulse at appropriate resonance angle and WFR velocity, as shown in Fig. 13(b). Since the SPP pulses with ultrashort duration have a higher temporal resolution, it may be potentially applied in the fields of ultrafast photoswitch and modulator.^[83,84] This technology is of great guiding significance, as it laid a theoretical foundation for generating nearly single-cycle femtosecond SPP pulse.

4.6. Micro-nano fabrication of femtosecond SPP

Based on the unique feature of ultrahigh peak power, femtosecond laser pulses can be used to modify the surface property of materials, such as metals, semiconductors and dielectrics, to form the plasmonic interface that supports SPP excitation and propagation.^[85–87] Affected by the scattering of nano-defects or NPs randomly distributed on the material surface, only a small portion of scattering wave of the incident laser pulse can satisfy the wave vector matching condition and then generate femtosecond SPP propagating along the material interface. Consequently, the excited femtosecond SPP interferes with the incident light to form interference fringes, resulting in a periodically discrete distribution of the laser energy within the beam spot area, *i.e.*, to form the multiple nanoscaled periodic heat sources. The absorption and deposition of the laser energy on material surfaces is a complex ultrafast dynamic process, which includes electronic thermalization, hot electron-cold lattice non-equilibrium formation, transient refraction index grating formation, electron-lattice energy transfer, and lattice fusion and removal, *etc.* When the incident laser energy is close to the ablation threshold of the material, one-dimensional (1D) subwavelength periodic grating-like structures, so-called ripples, will be formed within the laser irradiation area. The periodicity of the ripple structure depends on the excited SPP wavelength, while its orientation relies on the direction of SPP wave vector. Some research results have shown that both the wavelength and the

propagation direction of the femtosecond SPP excited on the material surface can be respectively altered by the wavelength and the polarization of the incident femtosecond laser pulse, so that the spatial periodicity and orientation of the ripple structure can be effectively manipulated.^[88–91] In 2008, Guo *et al.* reported using femtosecond laser pulses (65 fs, 1 kHz) respectively at the central wavelength of 400 nm and 800 nm successfully achieved femtosecond SPP waves on tungsten via modifying the transient optical property of the material surface, and finally imprinted the periodic ripple structures with period of 289 nm and 542 nm on the tungsten surface,^[88] as shown in Fig. 14(a). In 2012, Yang *et al.* manipulated the propagation direction of the femtosecond SPP wave excitation on copper surface by changing the long-axis direction of elliptically polarized femtosecond laser pulses (800 nm, 50 fs, 1 kHz),^[89] so as to continuously adjust orientation of induced ripple structures, as shown in Fig. 14(b). In 2012, Lou *et al.* employed a femtosecond vector beam (806 nm, 35 fs, 1 kHz) to generate different types of femtosecond vector SPP on the surface of silicon, and fabricated complex 2D subwavelength periodic structures (argument and radial patterns),^[90] as shown in Fig. 14(c). Additionally, other experimental parameters such as the pulse overlapping, the laser energy and fabrication environment should also be taken into account for manipulation of the wavelength of femtosecond SPP excitation on material surfaces so as to effectively manipulate the periods of the induced structure.^[91,92]

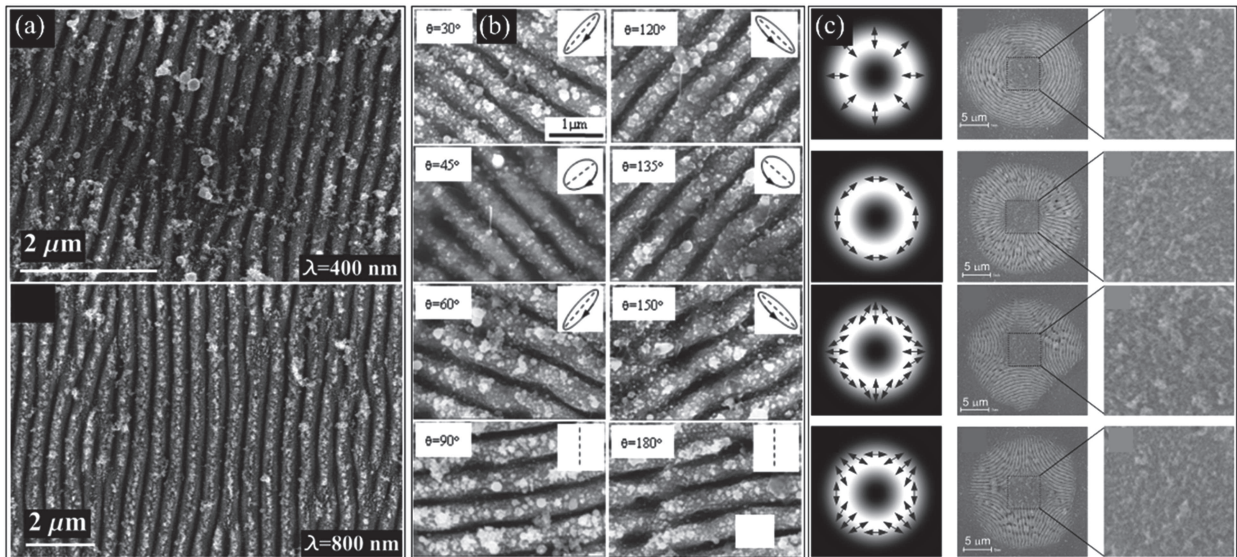


Fig. 14. (a) Fabricating 1D subwavelength periodic ripple structures on tungsten surface by femtosecond SPP with different wavelengths.^[88] (b) Controlling the orientation of the 1D subwavelength periodic ripple structures on copper surface by changing the wave vector direction of femtosecond SPP.^[89] (c) Fabricating the 2D subwavelength periodic structures on silicon surface by femtosecond SPP with optical vector field.^[90]

Recent research progresses suggest that the incident multiple femtosecond laser pulses with certain time delays can perform transient correlation behavior via exciting ultrafast nonequilibrium dynamics of material surfaces, in other words, the femtosecond SPP excitation of the time-delayed incident

laser pulses can be manipulated by the transient optical properties of the material surface pumped by the previously incident pulses, so as to realize the fabrication and flexible manipulation of two-dimensional (2D) subwavelength periodic surface structures.^[93–96] Yang's group achieved rapid one-step fabri-

cation of 2D subwavelength periodic surface structures, including rectangular,^[93] circular,^[94] and triangular array^[95] on the surfaces of molybdenum, tungsten and other materials by using time delayed double femtosecond lasers (50 fs, 1 kHz) with orthogonal linear polarizations at single-color (800 nm, 800 nm) or two-color (800 nm, 400 nm) wavelengths. Effective manipulation of orientation, cell size and spatial period of the 2D microstructures were realized by altering the polarization direction and inter-pulse delay time of the incident two femtosecond laser beams. Similarly, Fraggelakia *et al.* fabricated sub-micron triangular and rectangular array

structures on stainless steel surface by using temporally delayed dual femtosecond laser beams (1030 nm, 2 MHz, 350 fs) with circularly/linearly polarized configurations.^[96] The 1D and 2D subwavelength periodic surface structures fabricated by femtosecond SPP can have special interactions with visible to NIR lights, contributing to various applications such as the generation of structural colors,^[89] SERS,^[97] enhancement of absorption and thermal radiation,^[95,98] and photoelectron excitation efficiency.^[99] It is extremely valuable in the fields of biomimetic, anti-fake, biosensing, photoelectric detection, photovoltaic devices, and thermal radiation devices, *etc.*

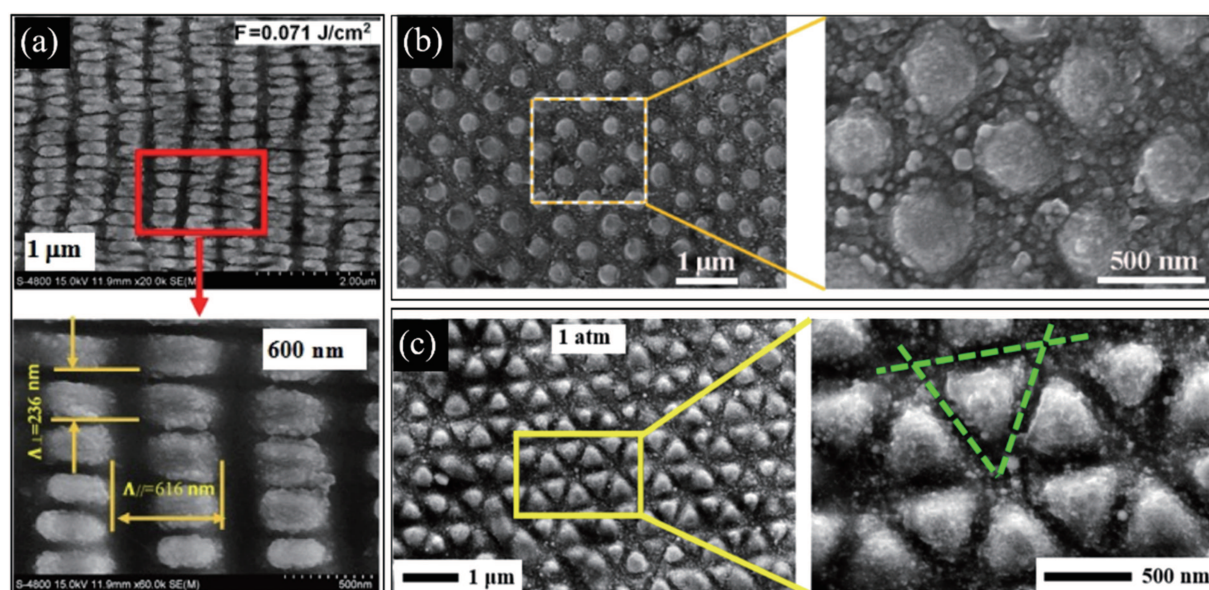


Fig. 15. (a) Fabricating 2D subwavelength rectangle array on Molybdenum surface based on the SPP excitation under irradiation of two-color temporally-delayed femtosecond laser pulses.^[93] (b)–(c) Fabricating 2D subwavelength circle and triangle array on Tungsten surface based on the SPP excitation under irradiation of temporally-delayed femtosecond laser double pulses.^[94,95]

5. Conclusion and perspectives

In this paper, the research progress of femtosecond SPP in recent years is briefly introduced and analyzed from two aspects: characteristic and application. Femtosecond SPP pulses provide an effective solution for researching ultrafast process and nonlinear signal enhancement occurring in extremely small spatiotemporal scale, due to its characteristics of femtosecond-scale temporal resolution, nanoscale spatial resolution, as well as near-field enhancement and ultrahigh peak power, which will lead to greater developments of many novel applications. For example, the ability of super spatiotemporal resolution of femtosecond SPP imaging can be utilized to the investigation and detection of single-molecule motion, SRS, and electron transport in optoelectronic chips. In addition, the ultra-high EM field enhancement ability of femtosecond SPP can also be used in the fields of single-molecule Raman detection, optical micro-/nanoscale manipulation, nanoscale light source and EUV pulse generation. With the further de-

velopment and improvement of femtosecond SPP research, it will bring profound influences on many fields such as nanophotonics, molecular dynamics and biomedicine.

Acknowledgment

The scientific contributions from other people or groups are acknowledged here. Financial supports are given in the footnote on the first page.

References

- [1] Ebbesen T H, Lezec H J, Ghaemi H F, Thio T and Wolff P A 1998 *Nature* **391** 667
- [2] Barnes W L, Dereux A and Ebbesen T W 2003 *Nature* **424** 824
- [3] Miyazaki H T and Kurokawa Y 2006 *Phys. Rev. Lett.* **96** 097401
- [4] Ciraci C, Hill R T, Mock J J, Urzhumov Y, Fernández-Domínguez A I, Maier S A, Pendry J B, Chilkoti A and Smith D R 2012 *Science* **337** 1072
- [5] Kim S, Jin J, Kim Y J, Park I Y, Kim Y and Kim S W 2008 *Nature* **453** 757
- [6] Kneipp K, Wang Y, Kneipp H, Perelman L T, Itzkan I, Dasari R R and Feld M S 1997 *Phys. Rev. Lett.* **78** 1667

- [7] Li J F, Huang Y F, Ding Y, Yang Z L, Li S B, Zhou X S, Fan F R, Zhang W, Zhou Z Y, Wu D Y, Ren B, Wang Z L and Tian Z Q 2010 *Nature* **464** 392
- [8] Du L P, Lei D Y, Yuan G H, Fang H, Zhang X, Wang Q, Tang D Y, Min C J, Maier S A and Yuan X C 2013 *Sci. Rep.* **3** 3064
- [9] Shen J F, Wang J, Zhang C J, Min C J, Fang H, Du L P, Zhu S W and Yuan X C 2013 *Appl. Phys. Lett.* **103** 191119
- [10] Pettinger B, Schambach P, Villagómez C J and Scott N 2012 *Ann. Rev. Phys. Chem.* **63** 379
- [11] Treffer R, Bohme R, Deckert-Gaudig T, Lau K, Tiede S, Lin X M and Deckert V 2012 *Biochem. Soc. T* **40** 609
- [12] Steidtner J and Pettinger B 2008 *Phys. Rev. Lett.* **100** 236101
- [13] Zhang R, Zhang Y, Dong Z C, Jiang S, Zhang C, Chen L G, Zhang L, Liao Y, Aizpurua J, Luo Y, Yang J L and Hou J G 2013 *Nature* **498** 82
- [14] Zhong J H, Jin X, Meng L Y, Wang X, Su H S, Yang Z L, Williams C T and Ren B 2017 *Nat. Nanotechnol.* **12** 132
- [15] Zayats A V, Smolyaninova I I and Maradudin A A 2005 *Phys. Rep.* **408** 131
- [16] Dou X J, Min C J, Zhang Y Q and Yuan X C 2016 *Acta Opt. Sin.* **36** 1026004
- [17] Maier S A 2007 *Plasmonics: Fundamentals and Applications* (Springer Science + Business Media LLC) pp. 25–34
- [18] Kretschmann E and Raether H 1968 *Z. Naturforsch.* **23** 2135
- [19] Zhang K, Du C G and Gao J C 2009 *Acta Phys. Sin.* **66** 227302 (in Chinese)
- [20] Otto A 1968 *Z. Phys.* **216** 398
- [21] Hecht B, Bielefeldt H, Novotny L, Inoué Y and Pohl D W 1996 *Phys. Rev. Lett.* **77** 1889
- [22] Hornauer D, Kapitza H and Raether H 1974 *J. Phys. D: Appl. Phys.* **7** L100
- [23] Maiman T H 1960 *Nature* **187** 493
- [24] Spence D E, Kean P N and Sibbett W 1991 *Opt. Lett.* **16** 42
- [25] Nabekawa Y, Kuramoto Y, Togashi T, Sekikawa T and Watanabe S 1998 *Opt. Lett.* **23** 1384
- [26] Nisoli M, DeSilvestri S, Svelto O, Szpöcs R, Ferencz K, Spielmann C, Sartania S and Krausz F 1997 *Opt. Lett.* **22** 522
- [27] Adachi S, Ishii H, Kanai T, Ishii N, Kosuge A and Watanabe S 2007 *Opt. Lett.* **32** 2487
- [28] Matsubara E, Yamane K, Sekikawa T and Yamashita M 2007 *J. Opt. Soc. Am. B* **24** 985
- [29] Hannaford P 2000 *Femtosecond laser spectroscopy* (Boston: Springer) pp. 61–86
- [30] Yamanouchi K 2002 *Science* **295** 1659
- [31] Peterman E J G, Monshouwer R, Stokkum I H M V, Grondelle R V and Amerongen H V 1997 *Chem. Phys. Lett.* **264** 279
- [32] Keller E L, Brandt N C, Cassabaum A A and Frontiera R R 2015 *Analyt.* **140** 4922
- [33] Douhal A, Lahmani F and Zewail A H 1996 *Chem. Phys.* **207** 477
- [34] Point G, Brelet Y, Houard A, Jukna V, Milián C, Carbonnel J, Liu Y, Couairon A and Mysyrowicz A 2014 *Phys. Rev. Lett.* **112** 223902
- [35] Panagiotopoulos P, Whalen P, Kolesik M and Moloney J V 2015 *Nat. Photon.* **9** 543
- [36] Krausz F and Ivanov M 2009 *Rev. Mod. Phys.* **81** 163
- [37] Vozzi C, Calegari F, Ferrari F, Lucchini M, Silvestri S D, Svelto O, Sansone G, Stagira S and Nisoli M 2009 *Laser Phys. Lett.* **6** 259
- [38] Morimoto Y and Baum P 2018 *Nat. Phys.* **14** 252
- [39] Dudley J M, Finot C, Richardson D J and Millot G 2007 *Nat. Phys.* **3** 597
- [40] Kravtsov V, Ulbricht R, Atkin J M and Raschke M B 2016 *Nat. Nanotechnol.* **11** 459
- [41] Park I Y, Kim S, Choi J, Lee D H, Kim Y J, Kling M F, Stockman M I and Kim S W 2011 *Nat. Photon.* **5** 677
- [42] Jiang Y Q, Narushima T and Okamoto H 2010 *Nat. Phys.* **6** 1005
- [43] Zhang Y Q, Shen J F, Min C J, Jin Y F, Jiang Y Q, Liu J, Zhu S W, Sheng Y L, Zayats A V and Yuan X C 2018 *Nano Lett.* **18** 5538
- [44] Zhang N, Zhu X N, Yang J J, Wang X L and Wang M W 2007 *Phys. Rev. Lett.* **99** 167602
- [45] Nishiyama Y, Imaeda K, Imura K and Okamoto H 2015 *J. Phys. Chem. C* **119** 16215
- [46] Mårssell E, Losquin A, Svård R, Miranda M, Guo C, Harth A, Lorek E, Mauritsson J, Arnold C L, Xu H X, Huillier A L and Mikkelsen A 2015 *Nano Lett.* **15** 6601
- [47] Gorkhover T, Schorb S, Coffee R et al 2016 *Nat. Photon.* **10** 93
- [48] Yalcin S E, Wang Y and Achermann M 2008 *Appl. Phys. Lett.* **93** 101103
- [49] Sámson Z L, Horak P, MacDonald K F and Zheludev N I 2011 *Opt. Lett.* **36** 250
- [50] Kubo A, Onda K, Petek H, Sun Z J, Jung Y S and Kim H K 2005 *Nano Lett.* **5** 1123
- [51] Ogawa S, Nagano H, Petek H and Heberle A P 1997 *Phys. Rev. Lett.* **78** 1339
- [52] Fecher G H, Schmidt O, Hwu Y and Schönhense G 2002 *J. Electron. Spectrosc.* **126** 77
- [53] Rotermund H H 1997 *Sur. Sci. Rep.* **29** 265
- [54] Kubo A, Pontius N and Petek H 2007 *Nano Lett.* **7** 470
- [55] Zhang L X, Kubo A, Wang L M, Petek H and Seideman T 2011 *Phys. Rev. B* **84** 245442
- [56] Wang W H and Zhang N 2018 *Acta Phys. Sin.* **67** 247302 (in Chinese)
- [57] Rewitz C, Keitzl T, Tuchscherer P, Huang J S, Geisler P, Razinkas G, Hecht B and Brixner T 2012 *Nano Lett.* **12** 45
- [58] Lemke C, Leibner T, Evlyukhin A, Radke J W, Klick A, Fiutowski J, Hansen J K, Rubahn H G, Chichkov B N, Carsten Reinhardt and Bauer M 2014 *Nano Lett.* **14** 2431
- [59] Sun Q, Ueno K, Yu H, Kubo A, Matsuo Y and Misawa H 2013 *Light Sci. Appl.* **2** e118
- [60] Frank B, Kahl P, Podbiel D, Spektor G, Orenstein M, Fu L W, Weiss T, Hoegen M H V, Davis T J, Meyer zu Heringdorf F J and Giessen H 2017 *Sci. Adv.* **3** e1700721
- [61] Ropers C, Neacsu C C, Elsaesser T, Albrecht M, Raschke M B and Lienau C 2007 *Nano Lett.* **7** 2784
- [62] Neacsu C C, Berweger S, Olmon R L, Saraf L V, Ropers C and Raschke M B 2010 *Nano Lett.* **10** 592
- [63] Müller M, Kravtsov V, Paarmann A, Raschke M B and Ernstorfer R 2016 *ACS Photon.* **3** 611
- [64] Berweger S, Atkin J M, Xu X G, Olmon R L and Raschke M B 2011 *Nano Lett.* **11** 4309
- [65] Neacsu C C, Reider G A and Raschke M B 2005 *Phys. Rev. B* **71** 201402
- [66] Li J M, Tang P, Wang J J, Huang T, Lin F, Fang Z Y and Zhu X 2015 *Acta Phys. Sin.* **64** 194201 (in Chinese)
- [67] Spektor G, Kilbane D, Mahro A K, Frank B, Ristok S, Gal L, Kahl P, Podbiel D, Mathias S, Giessen H, Meyer zu Heringdorf F J, Orenstein M and Aeschlimann M 2017 *Science* **355** 1187
- [68] Novotny L and Hulst N V 2011 *Nat. Photon.* **5** 83
- [69] Nahata A and Linke R A 2003 *Opt. Lett.* **28** 423
- [70] Pu Y, Grange R, Hsieh C L and Psaltis D 2010 *Phys. Rev. Lett.* **104** 207402
- [71] Zhang Y, Grady N K, Orozco C A and Halas N J 2011 *Nano Lett.* **11** 5519
- [72] Hanke T, Cesar J, Knittel V, Trügler A, Hohenester U, Leitenstorfer A and Bratschkitsch R 2012 *Nano Lett.* **12** 992
- [73] Galanty M, Shavit O, Weissman A, Aharon H, Gachet D, Segal E and Salomon A 2018 *Light Sci. Appl.* **7** 49
- [74] Frontiera R R, Henry A, Gruenke N L and Duyn R P V 2011 *J. Phys. Chem. Lett.* **2** 1199
- [75] Roxworthy B J and Toussaint Jr K C 2012 *Sci. Rep.* **2** 752
- [76] Kotsifaki D G, Kandyla M and Lagoudakis P G 2016 *Sci. Rep.* **6** 26275
- [77] Shoji T, Saitoh J, Kitamura N, Nagasawa F, Murakoshi K, Yamauchi H, Ito S, Miyasaka H, Ishihara H and Tsuboi Y 2013 *J. Am. Chem. Soc.* **135** 6643
- [78] Joly A G, Gong Y, El-Khoury P Z and Hess W P 2018 *J. Phys. Chem. Lett.* **9** 6164
- [79] Mittal R, Glenn R, Saytashev I, Lozovoy V V and Dantus M 2015 *J. Phys. Chem. Lett.* **6** 1638
- [80] Vogelsang J, Hergert G, Wang D, Groß P and Lienau C 2018 *Light Sci. Appl.* **7** 55
- [81] Toma K, Masaki K, Kusaba M, Hirokawa K and Kannari F 2015 *J. Appl. Phys.* **118** 103102
- [82] Pisani F, Fedeli L and Macchi A 2018 *ACS Photon.* **5** 1068
- [83] MacDonald K F, Sámson Z L, Stockman M I and Zheludev N I 2009 *Nat. Photon.* **3** 55
- [84] MacDonald K F and Zheludev N I 2009 *Laser Photon. Rev.* **4** 562
- [85] Vorobyev A Y and Guo C L 2013 *Laser Photon. Rev.* **7** 385

- [86] Huang M, Zhao F, Cheng Y, Xu N and Xu Z Z 2009 *ACS Nano* **3** 4062
- [87] Wang L, Chen Q D, Cao X W, Buividas R, Wang X W, Juodkakis S and Sun H B 2017 *Light Sci. Appl.* **6** e17112
- [88] Vorobyev A Y and Guo C L 2008 *J. Appl. Phys.* **104** 063523
- [89] Tang Y F, Yang J J, Zhao B, Wang M W and Zhu X N 2012 *Opt. Express* **20** 25826
- [90] Lou K, Qian S X, Wang X L, Li Y G, Gu B, Tu C H and Wang W T 2012 *Opt. Express* **20** 120
- [91] Shen M Y, Carey J E, Crouch C H, Kandyla M, Stone H A and Mazur E 2008 *Nano Lett.* **8** 2087
- [92] Xue L, Yang J J, Yang Y, Wang Y S and Zhu X N 2012 *Appl. Phys. A* **109** 357
- [93] Cong J, Yang J J, Zhao B and Xu X F 2015 *Opt. Express* **23** 5357
- [94] Qiao H Z, Yang J J, Wang F, Yang Y and Sun J L 2015 *Opt. Express* **23** 26617
- [95] Liu Q, Zhang N, Yang J J, Qiao H Z and Guo C L 2018 *Opt. Express* **26** 11718
- [96] Fraggelakis F, Mincuzzia G, Lopez J, Hönninger I M and Kling R 2019 *Appl. Sur. Sci.* **470** 677
- [97] Buividas R, Stoddart P R and Juodkakis S 2012 *Ann. Phys-Berlin* **524** L5
- [98] Vorobyev A Y, Makin V S and Guo C L 2009 *Phys. Rev. Lett.* **102** 234301
- [99] Hwang T Y, Vorobyev A Y and Guo C L 2009 *Phys. Rev. B* **79** 085425